Shedding light on processes that control particle export and flux attenuation in the twilight zone of the open ocean

Ken O. Buesseler,[a],[*] and Philip W. Boyd[b]

[a] Woods Hole Oceanographic Institution, Department of Marine Chemistry and Geochemistry, Woods Hole, Massachusetts
[b] National Institute of Water and Atmospheric Research, Centre for Chemical and Physical Oceanography, Department of Chemistry, Dunedin, New Zealand

Abstract

Pelagic food webs drive a flux of $>10 \times 10^{12}$ kg C yr^{-1} that exits surface waters, mostly via sinking particles through the ocean's "biological pump." Much of this particle flux is remineralized in the poorly studied waters of the twilight zone, i.e., the layer underlying the euphotic zone and extending to 1000 m. We present a reanalysis of selected upper-ocean studies of particulate organic carbon (POC) flux and relate these observations to a simple one-dimensional biological model to shed light on twilight zone processes. The ecosystem model first predicts particle flux from the base of the euphotic zone, and then its attenuation below based on transformations by heterotrophic bacteria and zooplankton, and active downward transport of surface-derived particles by zooplankton. Observations and simulations both suggest that future sampling strategies for the twilight zone should take regional variability of the euphotic zone depth (Ez) into account. In addition, conventional curve-fitting of particle flux data (i.e., power law or exponential) skews our interpretation of twilight zone processes. To overcome these artifacts, we introduce two new terms: the Ez-ratio (POC flux at Ez relative to net primary production [NPP]) and T_{100} (the ratio of POC flux 100 m below Ez to POC flux at Ez). A comparison of NPP, Ez-ratios, and T_{100} provides a new set of metrics to classify the ocean into different regimes, representing high and low surface export and subsurface flux attenuation.

The ocean's "twilight zone" is defined as the layer below the sunlit euphotic zone extending to depths of about 1000 m. The use of this term dates back to at least Russell (1931) and colleagues, who were interested in controls on the vertical distribution of marine macroplankton. The concept of sinking particles raining through this layer to the deep sea is also not new, as Agassiz (1888) and others explored deep-sea organisms and their nourishment from above. However, the advent of modern sediment trapping to intercept and capture the flux of settling ocean particles began much later, in the 1960s–1970s (Berger 1971; Honjo 1976; Soutar et al. 1977). Sediment traps allowed assessment of the relationship among surface algal productivity, particle export, and attenuation through the twilight zone (Berger et al. 1989). In addition to sinking particles, mixing of labile dissolved organic matter below depths that are seasonally ventilated, and the active transport of material by diel and seasonally migrating zooplankton form a complex system referred to as the "biological pump" (Volk and Hoffert 1985).

Many processes set the export flux out of the euphotic zone and determine attenuation of this flux through the twilight zone, i.e., the strength and efficiency of the biological pump. Since many of these processes are predominantly biologically controlled, the magnitude and attenuation of particle transport will vary with depth, season, and with regional variations in ecosystem structure. To understand this variability, relationships have been sought among food-web structure and retention and export of biogenic matter (Peinert et al. 1989). Many studies began with determining simple empirical relationships among

algal production, export, and particle flux through the twilight zone in both the open ocean (Suess 1980; Pace et al. 1987; Berger et al. 1988) and coastal seas (Wassmann 1990).

In the 1990s, progress continued in understanding ocean biogeochemistry through major programs such as the Joint Global Ocean Flux Study (JGOFS) (Fasham 2003), though sampling coverage of processes within the twilight zone in JGOFS was poor relative to both euphotic-zone biogeochemical processes and deep-water geochemical fluxes (Boyd and Trull 2007). Current knowledge of the factors that determine vertical decreases in particle flux through the twilight zone is based largely upon either examination of particle properties in deep traps (i.e., >1000 m depth; Honjo et al. 2008) or global application of a single parameterization of the particle flux vs. depth relationship (Martin et al. 1987). Alternatively, particle properties (i.e., mineral ballast) from deep traps have been linked to surface-ocean processes without a direct estimate of flux in between these strata (Francois et al. 2002; Klaas and Archer 2002). Another approach has been to combine flux estimates from multiple methods—remote sensing, upper-ocean budgets, new production and traps—to look at global variability in, and empirical relationships between, deep flux and surface-ocean properties (Lutz et al. 2002; Dunne et al. 2005).

The twilight zone has been understudied in part due to the many technical challenges associated with sampling these waters (Gardner 2000; Boyd and Trull 2007; Buesseler et al. 2007*a*). These challenges and undersampling of the twilight zone in general have conspired to limit understanding of transport of sinking particles through this layer. Recent advances in sampling particle flux in the twilight zone with free-vehicles, i.e., neutrally buoyant

* Corresponding author: kbuesseler@whoi.edu

sediment traps (NBSTs) (Valdes and Price 2000; Lampitt et al. 2008), have begun to add more measurements of flux vs. depth in this stratum. The recent VERTIGO (VERtical Transport In the Global Ocean) project set out to focus on the open-ocean twilight zone. During VERTIGO, concurrent measurements were made of sinking fluxes with NBSTs and biological processes in the surface and twilight zone that are important in particle formation, flux, attenuation, and active transport (Buesseler et al. 2008*b*). VERTIGO observations revealed significant regional variability in particle flux attenuation (Buesseler et al. 2007*b*); a higher fraction of net primary production (NPP) reaches deeper depths (to 500 m) in the northwest Pacific compared to the subtropical Pacific gyre. Key particle-transformation processes, such as the roles of heterotrophic bacteria and zooplankton in flux attenuation, were studied (Steinberg et al. 2008*b*), as well as the degree of coupling between surface planktonic community structure and twilight zone particle fluxes (Boyd et al. 2008). There is variability in the particle remineralization length scales of different major and minor components of export flux (Lamborg et al. 2008) and, critically, convergence in the magnitude of regional fluxes estimated by both sediment traps (NBSTs) and thorium-234 methods (Buesseler et al. in press).

Insights gained from VERTIGO have given us confidence in conducting both a retrospective analysis of selected open-ocean studies (Table 1) and in developing a simple one-dimension (1-D) biological model that simulates export from the euphotic zone and attenuation below. The objective was to select open-ocean sites (>1000-m water depth) with enough data on both geochemistry and biology to quantify and parameterize flux processes. Some of the biological rates desired included size-fractionated NPP, bacterial production, and zooplankton grazing. To obtain a standardized flux data set in the upper twilight zone, we chose studies where the naturally occurring tracer thorium-234 (^{234}Th) could be used as a proxy for the flux of particulate organic carbon (POC) in the open ocean (Benitez-Nelson and Moore 2006). This approach required depth-resolved ^{234}Th data and particulate POC : ^{234}Th ratios (*see* Methods) of sufficient data density to calculate POC flux vs. depth patterns.

In parallel to the data reanalyses, we developed a biological flux model that includes surface and subsurface components, where one set of parameters was used to derive POC flux at the base of the euphotic zone and another set of parameters was used to predict particle remineralization by heterotrophic bacteria, particle consumption by zooplankton, and the role of zooplankton in actively transporting POC to depth via vertical migration. Taken together, the simple surface and subsurface models capture the range of variability in the functioning of the biological pump evident from our selected observations. As more data become available on the twilight zone, our understanding of processes in this layer will increase and may warrant incorporation of more complexity into these models. At present, we use model sensitivity analyses to set constraints on the extent of biological processing of particles. We focus our attention on particle flux and

attenuation in the open ocean in an attempt to avoid the confounding factors affecting POC sources and sinks, such as terrestrial sources, lateral transport, benthic boundary layers, and more dynamic spatial variability in the coastal seas.

Together, the retrospective analysis of the POC flux data and model simulations are used to examine the consequence of sampling particle flux at a fixed depth at a range of open-ocean sites relative to the regional variability evident for euphotic-zone depths (which determine the vertical extent of NPP). This analysis and the modeling also set bounds on particle transformations and attenuation length scales within the twilight zone and form a conceptual model of a layered ocean with net particle formation in the euphotic zone and particle transformations below. What results from this exercise is not a comprehensive review of all particle flux data or a comparison between different flux methods. Instead, we use selected data to develop a new set of metrics to compare NPP and POC fluxes normalized to the depth of the euphotic zone, and relative flux attenuation below this reference horizon. These new metrics lead to recommendations for an improved framework for both sampling the twilight zone in future studies of the open ocean and subsequent data representation and classification. This approach will allow evaluation of the importance surface and subsurface processes that control the magnitude and efficiency of the biological pump at contrasting sites and seasons.

Methods

The need for normalization of fluxes to the depth of the euphotic zone—The findings of our study, from both reanalysis of observations and modeling simulations, lead us to advocate the normalization of particle fluxes to the depth of the euphotic zone, as opposed to absolute depth, and we use the abbreviation "Ez" as shorthand for the depth at the base of this stratum. Here, we provide, up front, the rationale and methodology for doing this, so that we can assemble comparable flux data that treat the ocean as a layered system. Within the upper layer, the "fuel" for the biological pump is mainly provided by phytoplankton production in the euphotic zone (most commonly defined by 1% or 0.1% light penetration; Jerlov 1968). Phytoplankton production fueled by vertical nutrient inputs from below the euphotic zone, so-called new production, is equivalent to export production relative to the same euphotic zone boundary, if averaged over suitable spatial and temporal scales (Eppley 1989). Below the euphotic zone, de novo production of particles by phytoplankton ceases, and heterotrophic bacterial and zooplankton processes interact to alter flux vs. depth patterns in the twilight zone.

Considering the ocean as a layered system is critical to studies of export to the twilight zone where euphotic-zone depths between sites can vary by >100 m and thus influence export flux sampled at a fixed depth (Boyd and Newton 1999). At the sites considered in our study, the euphotic zone ranges from 30 m (KIWI-7) to 125 m (ALOHA-A Long-term Oligotrophic Habitat Assessment).

Table 1.   Summary of POC fluxes.

ID	Depth (m)	POC flux[*] (mg m^{-2} d^{-1})	C:Th[†] (μmol:1/60 Bq)	NBST[‡]	Comments and references[§]
K2-D1	50	133	8		C:Th from >53–350 μm filter at 50 m, from
47°N, 160°E	150	53	3.9	62	NBST >50 m; ^{234}Th flux steady-state
July 2005	300	34	2.5	47	model for D1, 4 station avg.; Buesseler et
	500	23	1.7	29	al. (2008b, in press); NBST fluxes from
					Buesseler et al. (2007b)
K2-D2	50	39	8		Same as for K2-D1 except ^{234}Th non-steady-
47°N, 160°E	150	21	3.9	23	state model used
Aug 2005	300	13	2.5	17	
	500	9	1.7	13	
ALOHA	150	14.5	5.4	18	C:Th from NBST ^{234}Th flux steady-state
22°N, 158°W	300	5.6	2.1	6.6	model, 4 station avg.; Buesseler et al.
Jun–Jul 2004	500	4.3	1.6	3.6	(2007b, 2008b, in press)
NABE[‖]	50	493	18.3		C:Th from bottle POC and filter ^{234}Th
47°N, 20°W	150	600	11.9		(>1 μm); ^{234}Th flux non-steady-state
Apr–May avg. 1989	300	542	8.8		model; 4 station avg., Buesseler et al.
					(1992)
EQPAC	120	26	1.0		C:Th from >53 μm filters; ^{234}Th flux non-
0°N, 140°W	150	21	0.75		steady-state model, 2 station avg.; Bacon
Spring and fall avg. 1992	300	11	No data		et al. (1996)
KIWI-7	50	284	11.8		C:Th from >70 μm filters; ^{234}Th flux non-
61.5–65.5°S, 170°W	100	116	4.5		steady-state model S-APF avg. 5 stations;
Dec 1997	150	69	3.4		Buesseler et al. (2001, 2003)
KIWI-8	50	488	15.7		Same as for KIWI-7, 3 station avg.
61.5–65.5°S, 170°W	100	346	7.8		
Jan 1998	150	387	7.3		
OSP-May	50	31	4.8		C:Th from bottle POC and filter ^{234}Th;
50°N, 145°W	100	14	1.8		^{234}Th flux steady-state model, single
May 1996	150	9.6	1.4		station; Charette et al. (1999)
	200	8.3	0.9		
OSP-Aug	50	97	8.1		Same as for OSP-May
50°N, 145°W	100	36	2.3		
Aug 1996	150	31	No data		
	200	22	1.2		

[*] POC fluxes were derived from Th flux and C:Th ratios.
[†] C:Th ratios are reported in units of μmol : 1/60 Bq (1 Bq = 60 dpm = 60 disintegration per minute).
[‡] NBST, neutrally buoyant sediment trap fluxes as reported in Buesseler et al. (2007b).
[§] Comments on thorium flux model, C:Th ratios, and original references for all data.
[‖] In NABE, the "high" POC flux estimate from C:Th ratios derived from POC from bottle filtration was used (vs. traps; Buesseler et al. 1992), given the closer agreement with nutrient and other budgets.

If the particle flux out of the euphotic zone and the rates of particle remineralization below were identical at both sites, a considerably lower flux would be found in a trap at a fixed depth of 150 m at KIWI-7 relative to ALOHA due to additional particle transformations in the 95 m below the euphotic zone at KIWI-7 vs. only 25 m below the euphotic zone for ALOHA.

Further justification for the normalization of particle fluxes to the depth of the euphotic zone comes from recent high-vertical-resolution ^{234}Th studies, where the shallow ^{234}Th deficit (^{234}Th < ^{238}U activity) coincides with productive waters of the euphotic zone, while immediately below the euphotic zone, there can be a layer of ^{234}Th-excess (^{234}Th > ^{238}U), indicating net particle remineraliza-tion (Buesseler et al. 2008a). This concept of a layered ocean defined by a particle production layer above and flux attenuation below is not new (Bishop 1989; Boyd and Newton 1999; Wassmann et al. 2003), but it points to the

more explicit need for standardization of sampling depths relative to the euphotic zone across different oceanic regions and hence across different research programs. In practice, the exact way in which those layers are defined needs community input and consensus (1% or 0.1% light penetration, depth of NPP, depth where production = consumption, temporal averaging for the euphotic zone), but this concept is often ignored when designing sediment-trapping programs that collect samples at fixed depth, and particle flux data are interpreted based upon relative changes in flux at the same absolute depths. By normalizing fluxes to the euphotic zone, we can thus separate e-ratios, loosely defined in many prior studies as the particle flux at some arbitrary fixed depth divided by NPP (Murray et al. 1989), from what we term here "Ez-ratios," which are specific to the export flux at the euphotic zone divided by NPP (Ez-ratio = POC flux at Ez:NPP). If one is measuring particle flux deeper than the euphotic zone, as

is common, e-ratios would be less than Ez-ratios (assuming a decreasing POC flux vs. depth), and new production in the euphotic zone and the particle flux at deeper depths would not balance.

Determination of shallow POC flux profiles using thorium-234—The use of ^{234}Th as a particle flux proxy has recently been reviewed and synthesized (Benitez-Nelson and Moore 2006). In essence, ^{234}Th is a relatively short-lived ($t_{1/2} = 24.1$ d), particle-reactive tracer produced at a constant rate from its conservative and long-lived parent, ^{238}U. The broader application of ^{234}Th began with the JGOFS program in the late 1980s (Buesseler et al. 1992) and has expanded considerably to include many different sites (Waples et al. 2006) and important improvements in sampling and analysis (Rutgers Van Der Loeff et al. 2006), ^{234}Th flux modeling (Savoye et al. 2006), and assessment of POC:^{234}Th ratios and variability thereof (Buesseler et al. 2006; Santschi et al. 2006).

The ^{234}Th data considered in our reanalysis of open-ocean twilight zone data sets came from a limited number of research groups using a similar sampling and analytical protocol when making flux predictions, and the studies were all conducted as part of larger programs where ancillary biogeochemical information was readily available (VERTIGO, JGOFS, and Ocean Station Papa [OSP]; Table 1). Thus, comparative differences can be expected to be more robust than had we combined different approaches and compared different flux methods. We were also limited in our choice of flux data by the relatively poor vertical resolution, in the twilight zone, of prior studies for both ^{234}Th activities and POC:^{234}Th ratios, as their focus was usually on flux at a single, fixed depth (e.g., 100 m) rather than on POC flux vs. depth (Buesseler et al. 1995, 1998). Since errors in the ^{234}Th deficit increase with depth, this tracer is best applied to predict POC flux out of the euphotic zone and through the upper twilight zone (100–300 m below Ez). Here, we used existing data sets to recalculate the average POC flux profiles and take into account site-specific variations in Ez when examining particle flux out of the surface and attenuation below.

We reevaluate neither the assumptions and uncertainties in the ^{234}Th approach nor assumptions for other rates, such as NPP, but we refer the reader to published methods and synthesis papers (Knap et al. 1997; Benitez-Nelson and Moore 2006). We can gain some confidence in the ^{234}Th approach given evidence of similar NBST and ^{234}Th-derived fluxes of POC in the VERTIGO program (Table 1). In VERTIGO, both traps and ^{234}Th were used in time-series mode to capture the different spatial and temporal sampling scales of both methods (Buesseler et al. in press). It should be noted that traps, if deployed for a few days, integrate flux over smaller spatial scales and shorter time scales than ^{234}Th, which has a mean life of 35 d. Where possible, we used average ^{234}Th-derived fluxes (and NPP, which is derived mainly from 24-h incubations) from multiple stations to compare production and POC fluxes (sampling details in Table 1). In JGOFS, ^{234}Th-derived POC fluxes generally agreed with export estimates derived from nutrient and C budgets when compared over

appropriate spatial and temporal scales (*see* Figure 9 in Buesseler et al. 2006).

Biological modeling of surface export and the flux of POC through the twilight zone—We apply two simple modeling schemes. One model estimates downward POC export flux from the base of the euphotic zone, and the second model explores the relationship between POC flux attenuation and the interplay between three distinct biological processes that largely determine particle transformations within the twilight zone. The model that predicts POC flux out of the euphotic zone is based on a surface food web–particle export model (Michaels and Silver 1988). In brief, NPP is partitioned into different phytoplankton size classes, and this carbon is subsequently transferred, using prescribed trophic transfer efficiencies, through a pelagic food web (Fig. 1). Subsequently, a proportion of this NPP is exported (either directly [algal] or indirectly [fecal]) into the twilight zone (Fig. 1). This approach has been used previously to successfully predict POC export for a range of oceanographic provinces (Boyd and Newton 1995, 1999; Boyd et al. 2008). Modifications and improvements have been made, including employing the model under non-steady-state conditions (Boyd and Newton 1995), relating it to POC flux estimates at depths >1 km (Boyd and Newton 1999), and better constraining the proportion of NPP from microplankton that sinks directly relative to that grazed by mesozooplankton—the algal:fecal particle ratio (Boyd et al. 2008). In the present study, we use the model version detailed in Boyd et al. (2008), referred to hereafter as the "surface model."

The twilight zone flux-attenuation model predicts trends in downward POC flux (here to 500-m depth to match POC flux data) and explores how different biological processes alter the resulting particle flux profile (Fig. 1). Three processes are considered in the subsurface model: continuous solubilization of sinking particles by attached bacteria (Ploug 2001; Ploug and Grossart, 1999); discrete transformations of particles by zooplankton grazers, e.g., the conversion of an amorphous heterogeneous particle into a relatively compact fecal pellet (Dagg 1993; Thibault et al. 1999); and a vertical shunt of POC to depth that cannot be further transformed by either grazers or by attached bacteria as it "sinks," for example, carbon delivered to depth within the gut of a diurnally vertically migrating zooplankter and then egested as a fecal pellet, resulting in a source of new POC flux at depth (Wilson et al. 2008).

These three mechanisms operate in different ways and can be parameterized by observations of the environmental conditions in the twilight zone and understanding of heterotrophic processes (Table 2). Bacterial solubilization acts continuously as the particle settles (assuming that a large proportion of heterotrophic bacteria remain attached to the particle). To constrain the proportion of the POC flux that is solubilized by attached bacteria on the sinking particles, we require: information on rates of bacterial production (based on the thymidine incorporation method, which provide an estimate of net bacterial production by both free-living and attached bacteria; Kemp 1993); an estimate of the fraction of attached bacteria (25%) relative to
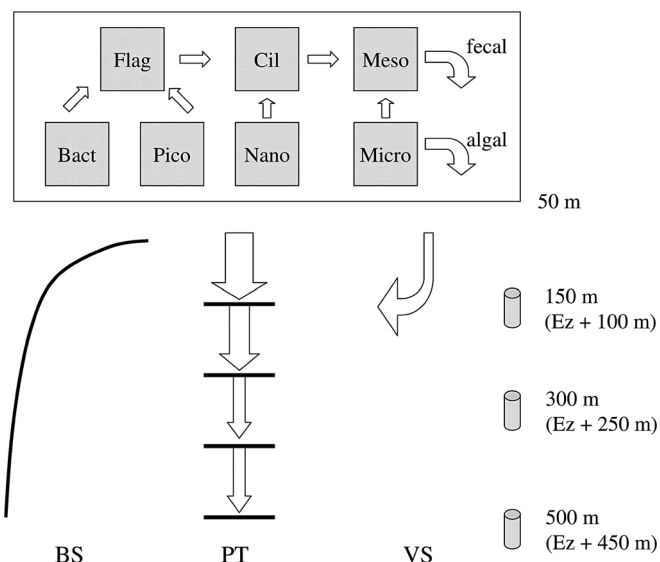
Fig. 1. A schematic of the two models that straddle the euphotic zone and the twilight zone. The export flux at the base of the euphotic zone is predicted using a surface food web–particle export model. NPP is partitioned into heterotrophic bacteria (Bact), picophytoplankton (Pico), nanophytoplankton (Nano), and microphytoplankon (Micro), which are consumed by heterotrophic flagellates (Flag), ciliates (Cil), and mesozooplankton (Meso), resulting in POC export as fecal and algal matter (Michaels and Silver 1988; Boyd et al. 2008). In the subsurface model, this export flux is subjected to bacterial solubilization as a continuous process (BS curve) and zooplankton particle transformations (PT arrows) and vertical migration (VS arrow to 100 m) as discrete processes parameterized by a set of length scales. Parameterization of these three processes is found in Table 2. These models are used to predict POC flux at the base of the euphotic zone and several depths below, shown here conceptually for a 50-m euphotic-zone depth and hypothetical traps at fixed depths of 150 m, 300 m, and 500 m.

the total (i.e., free-living and attached) bacterial abundances (Ploug 2001; Ploug and Grossart, 1999); and the ratio of gross (i.e., bacterial respiration + net bacterial production; Kemp 1993) to net bacterial production (4.0; Ploug 2001; Ploug and Grossart, 1999). Thus, rates of net bacterial production are equivalent to gross bacterial production by attached bacteria (net production $\times$ 0.25 $\times$ 4.0).

A comparison of column-integrated rates of net bacterial production with corresponding export fluxes in the twilight zone at four open-ocean sites (Table 3) indicates that around 30% of the export flux is consumed by bacterial solubilization, for an average POC flux transfer efficiency (TE) of 70%, which, for simplicity, is the default value at all depths (parameterized in the standard model as 30% POC loss per 150 m or 0.2% per m; Table 2). In later, modified model runs, we add depth dependence to this transfer efficiency, made evident by the range of bacterial solubilization rates vs. depth (Table 3, *see* for example K2).

We modeled attenuation of flux by a zooplanktonic particle feeder as a discrete process at a depth below Ez where specialist zooplankton groups reside (Dagg 1993), resulting in the production of a new particle with a given efficiency expressed as proportion of the sinking carbon

ingested that is egested as a fecal pellet (Thibault et al. 1999). Because we parameterized this particle transformation as a discrete process, we can represent it in the model as a particle-transformation (PT) length scale. Due to a lack of detailed published information on PT length scales, in the standard run, we arbitrarily set this to a flux-attenuation step, every 100 m below Ez (Table 2). Hence, each PT results in a new sinking particle being produced that retains 40% of the carbon prior to the transformation. The remaining 60% is attributed mainly to respiration and sloppy feeding, and to a lesser extent maintenance and growth (Straile 1997).

The employment of such a PT length scale mimics a sinking particle being intercepted by zooplankton groups that reside in different depth strata within the twilight zone (Fig. 1). It also permits analysis of the way in which discrete vs. continuous processes alter POC flux with depth. We use longer length scales to parameterize less particle consumption and hence less attenuation of export flux by zooplankton grazers. By default, the biogeochemical effects of aggregation of phytoplankton cells, which enhance the sinking of intact phytoplankton, are indirectly captured here by using a very long PT length scale. In this case, sinking POC does not pass through a zooplankton gut, but these aggregates would still be subjected in the model simulation to bacterial solubilization.

The vertical shunt (VS) of carbon by migrating zooplankton is the third process modeled, and it is the only one that can increase POC flux at depth. We approximate vertical migration by transporting a fraction of the POC flux (20 mg C m^{-2} d^{-1}; Table 2) out of the euphotic zone down to a fixed depth below the euphotic zone (100 m in our standard run; Table 2). This generic process that enhances flux at depth could also be used to represent any setting where suspended particles are repackaged to form new sinking particles at depth, such as by the mucous feeding webs of some larvaceans (Steinberg et al. 1997; Robison et al. 2005).

Default values for all of these mechanisms and rate estimates are provided in Table 2 with references. Because of the depth dependency of each process represented in this model, an example of the way fluxes in the standard run were calculated is provided in Table 4, rather than a conventional set of model equations. In this example, the model is used to calculate fluxes at 150, 300, and 500 m (the same depths resolved in VERTIGO traps) for conditions of Ez = 50 and 130 m. The flux is altered first by bacterial solubilization (0.2% m^{-1}), next by the vertical shunt (20 mg C m^{-2} d^{-1} added 100 m below Ez), and then by zooplankton particle transformations (60% lost at 100, 200, 300, and 400 m below Ez). In the sensitivity analysis, the values ascribed to these three processes are systematically varied (Table 2). This model is referred to hereafter as the subsurface model.

Results

Export flux out of the euphotic zone: Observations and simulations—In the selected studies, NPP ranges from 200 to 1400 mg C m^{-2} d^{-1}, and POC export at Ez ranges

Table 2.   Summary of the three biological processes, standard parameters, and sensitivity ranges used in the subsurface model.

Process	Mode	Standard run	References	Sensitivity analyses[*]
Bacterial solubilization (BS)	Continuous	0.7 transfer efficiency (TE)[†]; no depth dependence	Ducklow et al. (1993); Sherry et al. (1999); Boyd et al. (1999); Martin et al. (1993); Buesseler et al. (2007b); B. Van Mooy and P.W Boyd unpubl. data	TE 0.9 to 0.5; depth dependence increases or decreases with depth
Zooplankton particle transformation (PT)	Discrete	PT length scale 100 m[‡]; gross growth efficiency (GGE) 0.4[§]	Straille (1997)	PT 50 m to 300 m
Vertical migration shunt (VS)	Discrete	100 m shunt, 20 mg C m^{-2} d^{-1}[‖]	Boyd et al. (1999)	Shunt to 200 m, 0–60 mg C m^{-2} d^{-1}

[*] Sensitivity analyses shown in Fig. 4.
[†] TE is based on a comparison of column-integrated bacterial production (thymidine incorporation) in the twilight zone with column-integrated export + bacterial production, export flux corrected for bacterial solubilization, for four oceanic provinces, and assuming that TE is net BP, which is 0.25 of gross BP (BP + bacterial respiration) (Steinberg et al. 2008b) and that the BP of attached bacteria represents 0.25 of total (i.e., free-living vs. attached) BP (Ploug, 1991; Ploug and Grossart, 1999). TE = 1 − ([0.25BP/0.25]/[export flux + BP]). *See* Table 3.
[‡] Arbitrarily assigned for this study, but model sensitivity to this selection is tested.
[§] GGE = 0.4 from review by Straille (1997) of food-web transfer efficiencies in the mixed layer; in the absence of data for resident grazers in the twilight zone, we have assumed this efficiency in the model.
[‖] Based on vertical POC shunt at OSP based on net tows and fecal pellet production (Boyd et al. 1999).

from <20 to almost 500 mg C m^{-2} d^{-1} (Fig. 2). As a ratio to NPP, the ^{234}Th-derived Ez ratios vary from 2% to 45% (Table 5). Due to the need in our surface model for data on size-fractionated NPP and the algal:fecal ratio, we can estimate model-derived POC flux for only four of six sites. At these sites, agreement between the export flux derived from our model and a natural radionuclide tracer is encouraging (Fig. 2). For example, at the VERTIGO sites, K2 and ALOHA, as well as for the North Atlantic Bloom Experiment (NABE), the model and ^{234}Th-derived fluxes agree within 30%. At OSP, however, modeled export flux in May is more than twice the ^{234}Th-derived POC flux, but it is smaller for August (Table 5). One of the reasons for this mismatch may be that, unlike the other POC flux and NPP data, which are averages of multiple stations for VERTI-GO and NABE, the OSP data are from single profiles of

^{234}Th and NPP, which may introduce temporal mismatches between ^{234}Th (24-d half-life) and NPP (1-d incubation) results.

The highest observed Ez ratio is 45% for NABE (Table 5), consistent with a bloom that exports a large proportion of algal biomass directly (Honjo and Manganini 1993). Relatively high Ez ratios are also seen at stations just south of the Polar Front (Ez ratios of 29–34% for KIWI-7 and -8). This ecosystem was dominated by large diatoms and characterized by some of the highest daily rates of export production and annual average Ez ratios relative to other stations north of the Polar Front along the 170°W meridian (Buesseler et al. 2003). The Ez ratio in the NW subarctic Pacific was only slightly lower (25%) during deployment 1 (K2-D1), even though it was sampled ~50 d after the seasonal diatom productivity

Table 3.   Comparison of bacterial production rates and downward POC flux in four open-ocean sites.

Site	Depth (m)	BP	POC flux	BP/(BP + POC flux)
K2-D1	150 m	4.1	62	0.06
	300 m	21	47	0.31
ALOHA	150 m	16	18	0.47
	300 m	5.1	7.2	0.41
	500 m	1.6	3.6	0.31
NABE	50 m	321	600	0.35
	150 m	80	300	0.21
	300 m	40	200	0.17
OSP	100 m	30	67	0.31
	200 m	24	47	0.33
	500 m	13	19	0.40

All rates are in mg C m^{-2} d^{-1}.
BP denotes net bacterial production integrated over the overlying water column (i.e., 0–150 m; 150 to 300 m).
(BP + POC flux) is the amount of carbon available to the bacteria to solubilize as the particle sinks to the depth in the left-hand column.
BP/(BP + POC flux) provides an estimate of the proportion of the flux attenuation that is removed by bacteria.
Solubilization by attached bacteria accounts for ~30% of flux attenuation, so ~70% of the flux remains at each trap depth (in the standard model run, we arbitrarily assumed that 30% of the flux was attenuated between trap depths; i.e., TE = 70% per 150 m; 0.2% loss per m).
Data were obtained from the following sources: OSP (Boyd et al. 1999), NABE (Ducklow et al. 1993; Martin et al. 1993), K2 and ALOHA (B. Van Mooy unpubl. data; Buesseler et al. 2007b).

Table 4.   Example of subsurface model calculations with Ez = 50 and 130 m. Note the depth dependency of each process that prevents the model equations being listed conventionally in the main text.

Depth* (m)	Depth below Ez[†] (m)	Bacterial solubilization[‡]	Vertical shunt[§]	Particle transformation[‖]	Flux[¶] (mg C m^{-2} d^{-1})
Process		Continuous	Discrete	Discrete	
Formulation		0.2% every m	20 mg shunted to 100 m	60% loss at 100-m intervals	
50	0				100
150	100	(100) × 0.8	80 + 20	(80 + 20) × 0.4	40.0
300	250	(40) × 0.7	Na	(28) × 0.4	11.2
500	450	(11.2) × 0.6	Na	(6.7) × 0.4 × 0.4	1.1
130	0				100
150	20	(100) × 0.96	Na	Na	96.0
300	170	(96) × 0.7	67.2 + 20	(87.2) × 0.4	34.9
500	370	(34.9) × 0.6	Na	(20.9) × 0.4 × 0.4	3.3

* Absolute depth relative to surface.
[†] Depth below euphotic zone (Ez; example of 50 m [upper] and 130 m Ez [lower]).
[‡] BS reduces flux by 30% every 150 m, or 0.2% for every m, so loss is calculated from difference between Ez-normalized depths and this solubilization factor.
[§] VS adds 20 mg C m^{-2} d^{-1} at 100 m below Ez only, so it shows up in 100-m and 170-m depths for Ez = 50 and 130 m, respectively.
[‖] PT consumes 60% of the remaining flux at fixed layers 100 m below Ez and every 100 m thereafter, i.e., stepwise at 100, 200, 300, and 400 m below Ez (so can show up as two transformations if interval includes two steps, such as between 250 m and 450 m with Ez = 50 m).
[¶] Sum of flux at that depth.

maximum (Honda et al. 2006; Buesseler et al. 2008*b*). In the NW Pacific, the decrease in Ez ratio from deployment 1 to 2 (10 d later) was driven by a faster decrease in POC flux than in NPP over this period, consistent with an observed shift to a greater proportion of NPP by smaller algal cells (Boyd et al. 2008).

In the northeast subarctic Pacific, ratios were considerably lower, at least relative to the first occupation of the K2 site; Ez ratios were 3–14% using the POC flux data (Table 5) or about 8–9% if modeled export is used. Some of the lowest observed Ez ratios were from the subtropical and tropical Pacific sites of ALOHA (8%) and EQuatorial PACific (EQPAC) (2%), respectively. These systems have

relatively constant rates of NPP and are characterized by picoplankton and grazing thereon by microzooplankton (Landry et al. [1997] for EQPAC), and again our surface model and ^{234}Th data capture these differences by predicting low export production for such systems.

Particle flux attenuation: Mathematical fitting of POC flux vs. depth profiles—A number of early studies suggested that the best fit to the observed decrease in particle flux vs. depth was obtained using a depth-normalized power function (Martin et al. 1987; Pace et al. 1987; Berger et al. 1988). The most commonly used form is often referred to as the Martin curve:

$$F_z = F_{100}(z/100)^b, \qquad (1)$$

where F_z is the flux at depth z (m), F_{100} is the flux at 100 m (and the intercept in a log-log transformation), and b is the log-log slope. Martin et al. (1987) emphasized that this fitting did not parameterize a particular process but that this curve provided the best statistical fit for the range of VERtical Transport and EXchange (VERTEX) trap data (50–2000 m) with an average "open-ocean composite" b value for POC of -0.858 (b values ranging from -0.32 to -0.97 for individual profiles). When our POC flux data are treated in the same manner (Fig. 3a,c), the b values range from -0.27 to -1.29 (values, including standard error and F_{100}, are given in Table 6), where a more negative b indicates greater POC flux attenuation in the upper several hundred meters.

For twilight zone studies, we propose that application of the Martin curve has some important consequences for the interpretation of flux vs. depth patterns, and thus for the biogeochemical implications of apparent regional differences in flux attenuation. First, we note that as a power function, the curve approaches infinity at zero depth (*see* extrapolation of curves shallower than 100 m in Fig. 3a,c). Thus, comparisons between sites are very sensitive to
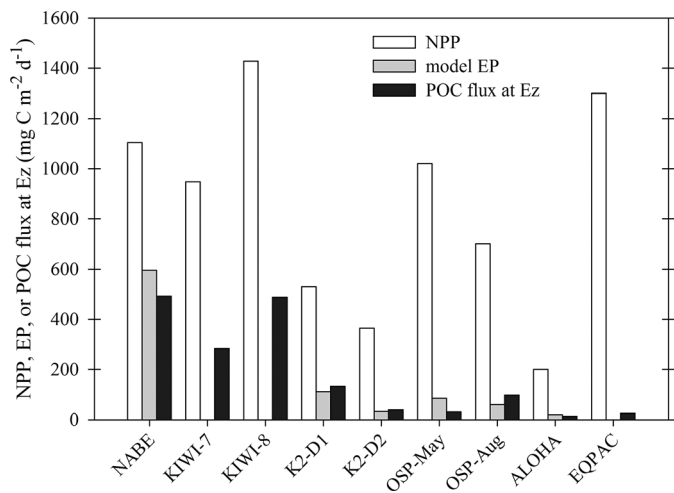

Fig. 2.   Bar plot for comparison of net primary production (NPP, white bar), surface model export flux at the base of the euphotic zone (gray bar), and POC flux derived from ^{234}Th (black bar) also at the base of the euphotic zone (all in units of mg C m^{-2} d^{-1}). The sites are listed in Table 1. The export flux was only able to be modeled at six of the nine sites. The ratio of POC flux at the base of the euphotic zone to NPP is called the Ez-ratio.

Table 5. Summary of euphotic-zone (Ez) depth, POC flux, NPP, Ez-ratio, T_{100}, and POC flux 100 m below Ez.

ID	Ez* (m)	Flux at Ez† (Th-derived; mg m⁻² d⁻¹)	Flux at Ez‡ (model; mg m⁻² d⁻¹)	NPP§ (mg m⁻² d⁻¹)	Ez-ratio Th‖	Ez-ratio model¶	T_{100} Th# (%)	T_{100} model** (%)	Flux 100 m below Ez†† (mg m⁻² d⁻¹)
K2-D1	50	133	111	530	0.25	0.21	40	67 avg	68
K2-D2	50	39	33	365	0.11	0.09	54		25
ALOHA	125	15	21	200	0.07	0.11	67	65	10
NABE	50	493	596	1104	0.45	0.54	>100	80	493
EQPAC	120	26		1300	0.02		61		16
KIWI-7	30	284		984	0.29		32		78
KIWI-8	60	488		1428	0.34		80		345
OSP-May	60	31	85	1020	0.03	0.08	31	16 avg	8
OSP-Aug	40	97	60	700	0.14	0.09	32		29

* Euphotic-zone depth defined by 0.1% light levels or depth as provided by original sources (Table 1) and averaged here for period under consideration.
† Thorium-234–derived POC fluxes from depth closest to the base of euphotic zone (Table 1).
‡ POC flux derived from food web–particle model described in this manuscript and as detailed in Boyd et al. (2008).
§ NPP, integrated primary production average as determined in original study.
‖ Ez-ratio, POC flux at Ez : NPP (extrapolated with closest ²³⁴Th-derived POC flux).
¶ Ez-ratio, POC flux at Ez : NPP (from surface model POC flux at Ez).
# T_{100} defined by ratio of POC flux 100 m below Ez : POC flux at Ez (fluxes extrapolated from linear fit to Fig. 5).
** T_{100} defined by ratio of POC flux 100 m below Ez : POC flux at Ez (fluxes from subsurface model; avg. of two deployments for K2 and OSP).
†† POC flux 100 m below Ez derived from a linear fit to ²³⁴Th-derived POC flux data (for NABE, we used T_{100} = 100% and Th-derived POC flux at Ez).

Table 6. Mathematical fits to POC flux vs. depth.

ID	Martin* b	± SE	F_{100} (mg m⁻² d⁻¹)	± SE	Exponential† z* (m)	± SE	F_0 (mg m⁻² d⁻¹)	± SE
K2-D1	−0.79	0.04	77	2	161	47	127	16
K2-D2	−0.61	0.02	26	1	244	54	37	4
ALOHA	−1.17	0.20	23	3	216	74	16	3
NABE	No fit		No fit		>1000			
EQPAC	−1.03	0.08	32	1	217	24	25	0.9
KIWI-7	−1.29	0.003	116	0.2	63	8	388	33
KIWI-8	−0.27	0.18	394	37	357	383	457	71
OSP-May	−1.05	0.07	15	1	78	20	30	3.5
OSP-Aug	−1.16	0.14	43	4	77	20	106	15

* Power-law fit of POC flux vs. depth data (Table 1) as proposed by Martin et al. (1987). Provided are the values of *b* and F_{100} from Eq. 1 and the standard error for each term (fit and error from SigmaPlot© power-law function; *n* = 3 to 4 as reported in Table 1). Fits all had R^2 > 0.95, except for KIWI-8 (R^2 = 0.66).
† Exponential fit of POC flux vs. depth data (Table 1) as proposed by Suess (1980) and reviewed by Boyd and Trull (2007). Provided are the values of z* and F_0 from Eq. 2 and the standard error for each term (fit and error from SigmaPlot© exponential decay function; *n* = 3 to 4 as reported in Table 1). Fits all had R^2 > 0.90, except for KIWI-8 (R^2 = 0.45).
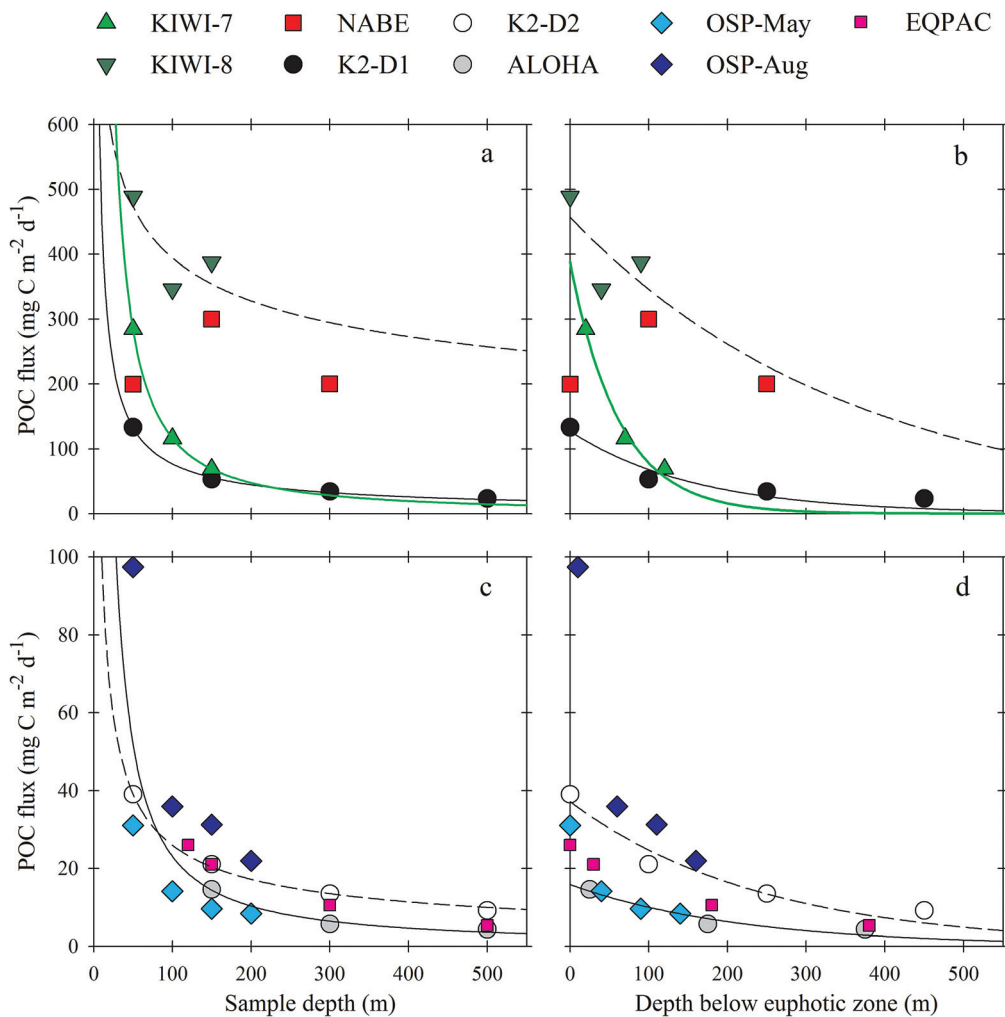
Fig. 3.   Plot of POC flux vs. depth and representative fits to the Martin curve (a, c) (Eq. 1; data plotted vs. sample depth) or exponential fit (b, d) (Eq. 2; data plotted vs. depth below euphotic zone). Data are from Table 1. The four high-flux sites are plotted in (a) and (b) on a POC flux scale of 0–600 mg C m^{-2} d^{-1}, while the five lower-flux sites are plotted in (c) and (d) on a flux scale of 0–100 mg C m^{-2} d^{-1}. In the upper panels, the best fit is drawn for KIWI-8 (dashed line), KIWI-7 (solid green line), and K2-D1 (solid black line). In the lower panels, the best fit is drawn for K2-D2 (dashed line) and ALOHA (solid black line). The mathematical fits and associated uncertainties for each site are provided in Table 6.

differences in sampling depths, particularly at shallow depths. For example, an ALOHA *b* value of −1.17 (standard Martin fit for flux at 150, 300, and 500 m; Table 6) would change for the same POC flux data to −0.45 if the data were plotted vs. depth below the euphotic zone (25, 175, 375 m for POC flux below Ez at this site). We contend that the process we are trying to understand, flux attenuation, should be evaluated based upon the flux relative to its depth below the layer of particle formation, the euphotic zone, and not an absolute depth in the water column. Hence, this sensitivity of the curve fit to shallow sample depths would introduce bias that is site-specific (i.e., dependent on Ez). Another potential artifact introduced by the Martin fitting routine was reported by Primeau (2006). He suggested that F_{100} and *b* are positively correlated, so as we move to sampling flux at shallower depths, i.e., higher fluxes, the resulting *b* values will be larger (more negative), implying higher remineralization in a system that does not necessarily have higher flux attenuation.

To introduce a more process-oriented parameterization of flux-attenuation processes, others have suggested using a first-order kinetic form of the flux vs. depth curve, where the rate of remineralization is proportional to the amount of material present and decreases exponentially with time (Suess 1980; Armstrong et al. 2002; Lutz et al. 2002). Since time can be reformulated based on the sinking rate and depth over which the particles are remineralized, this relationship can be simplified to:

$$F_z = F_0 \exp(z - z_0)/z^*, \qquad (2)$$

where z^* is the characteristic remineralization length scale for the flux decrease below z_0 (Boyd and Trull 2007). Data fitted in this format have a maximum at the reference depth z_0 (here using Ez as the reference depth), and the length scale does not change if plotted relative to a different reference horizon (i.e., z^* is the same whether plotting vs. absolute depth or depth relative to Ez).

Fits to Eq. 2 are plotted relative to Ez in Fig. 3b,d. The fit captures most of the shallow POC flux vs. depth pattern, resulting in remineralization length scales of 63 to >350 m (*see z* in Table 6; NABE data do not permit an accurate curve fit to either equation, since they suggest no attenuation in the upper 300 m). Prior studies have noted, however, that a single exponential length scale often results in a flux that decreases too quickly to fit deeper trap data (for example, as measured in deep-moored sediment traps >1000 m; Armstrong et al. 2002; Lutz et al. 2002). Indeed, in our study also, the POC flux data deeper than about 300 m are poorly fit by a single exponential curve. For example, a single exponential fit to the KIWI-7 POC flux profile suggests essentially zero flux by 300 m, yet it is reported that at least 1–2% of the POC flux reaches 1000 m or deeper at this site (Honjo et al. 2000; Nelson et al. 2002). This poorer fit to deeper flux data has been used to argue for the existence of at least two classes of sinking particles, one of which has a longer remineralization length scale (Armstrong et al. 2002; Lutz et al. 2002), resulting in separate F_0 and $z*$ values for at least two particle classes. In our study, since we only have three or four data points for any given site, we do not feel justified in defining a second exponential to better fit the flux data below 200 m, but rather we use a single exponential to compare the range in flux attenuation immediately below the euphotic zone between sites.

Particle flux attenuation: Modeled flux profiles—There are two standard subsurface model runs that result in a prediction of flux vs. depth, one for particles exiting a shallow euphotic zone (Ez = 50 m) and another with a deep euphotic zone (Ez = 130 m). In order to explore the relative effects of the three processes in the twilight zone, an export flux of 100 mg C m^{-2} d^{-1} was arbitrarily assigned to particles exiting each Ez (though in reality, the magnitude of this flux will vary depending upon NPP and the Ez-ratio). Flux data were modeled relative to an absolute sampling depth to examine the possible consequences of sampling particle flux at sites with different Ez values, while maintaining identical biological parameterizations in the twilight zone. A sensitivity analysis was then run to examine the effect on the vertical particle flux profile of varying each of the following parameters in our model (and keeping the remainder constant): the transfer efficiency of bacterial solubilization of particles (0.5 or 0.9 of the carbon is transferred; standard run uses TE = 0.7; continuous process); the length scale of a grazer-mediated particle transformation (50 m or 300 m; standard run uses PT = 100 m; discrete process); or the magnitude of a vertical shunt of carbon (0 or 60 mg C m^{-2} shunted to 200 m below Ez; standard run uses VS = 20 mg C m^{-2} d^{-1} to 100 m below Ez; discrete process).

The two standard runs (Fig. 4a) demonstrate that sites with different Ez values are sampled differently (and interpreted incorrectly) using the conventional scheme of sampling particle flux at fixed depths. The most obvious difference is that for the shallower Ez, there is more flux attenuation by a depth of 150 m. In this case, the predicted flux at 150 m is 40 mg C m^{-2} d^{-1} for Ez = 50 m and

96 mg C m^{-2} d^{-1} for Ez =130 m using the same biological parameters in the subsurface model. If fit using the Martin curve, the *b* value would change from −2.0 to −1.7 for Ez = 50 and 130 m, respectively (150, 300, and 500 m model fluxes are fit here). Put another way, attenuation appears greater (a more negative *b* value) with a shallow Ez and a flux profile sampled at a greater distance below the euphotic zone. Note that this discrepancy decreases with increasing depth (Fig. 4a), such that at depths >1000 m (i.e., the minimum depth often recommended for using deep bottom-moored traps; Buesseler et al. 2007*a*), the influence of these different Ez depths would not be an issue.

For our sensitivity analyses, we first altered only the bacterial transfer efficiency across a range from 0.5 to 0.9. This had relatively little effect on the particle flux at depth, e.g., for Ez = 50 m, flux at 150 m is 35 and 45 mg C m^{-2} d^{-1}, for TE = 0.5 and 0.9, respectively, vs. 40 mg C m^{-2} d^{-1} for the standard run (Fig. 4b). Also, the general shape of the resulting flux profile looks comparable to what is observed from ocean data sets, with an increase in the slope of flux vs. depth relationship for the lower transfer efficiency and a decrease for a higher transfer efficiency, for example, *b* = −2.5 for TE = 0.5, and *b* = −1.7 for TE = 0.9 (calculated for Ez = 50 m).

Alteration of the length scale of zooplankton PT had the largest effect of the three processes in this sensitivity analysis. If we compare a PT of 300 m and 50 m, the flux at 300 m drops from 70 to 1 mg C m^{-2} d^{-1}, respectively, for Ez = 50 m (vs. 11 mg C m^{-2} d^{-1} in the standard run). For Ez = 130 m, a change of PT from 300 m to 50 m reduces the 300 m flux from 87 to 6 mg C m^{-2} d^{-1}, respectively (vs. 35 mg C m^{-2} d^{-1} in the standard run) (Fig. 4c). In all of these cases, flux decreases with depth, but with different slopes. On the basis of the shape of the flux profile alone, one cannot determine which PT value is more reasonable.

In the sensitivity analysis of the VS, the shape of the curve does change and can exhibit an increase with depth when the upper bound for the VS shunt is used with a shallow Ez (for example, VS = 60 mg C m^{-2} at 200 m for Ez = 50 m; Fig. 4d). Such profiles might be interpreted as representing a mismatch between the particle source funnel and the traps intercepting particles below it, where the deeper trap is collecting flux from a source of higher POC export that is lateral to the trap site (Siegel and Deuser 1997). However, the VS is also a plausible way in which flux can increase with depth. Since such increases are not a common feature of most flux profiles in the twilight zone (Martin et al. 1987; Buesseler et al. 2007*b*), this implies at least in the open ocean that VS is not regularly as large or deep as suggested by this sensitivity run (here, our maximum VS was equivalent to 38% of the total C leaving the euphotic zone; = 60/[60 + 100]). In terms of absolute changes to flux at depth, altering the VS has less effect than changing PT length scales. Here, a shift from no carbon exported by the VS, our upper bound (60 mg C m^{-2} d^{-1} at 200 m), results in a change in the 500 m flux from 0.9 to 3.2 mg C m^{-2} d^{-1} with Ez = 50 m (vs. 1.1 mg C m^{-2} d^{-1} for the standard run), or for Ez = 130 m, 2.6 to 12.2 mg C m^{-2} d^{-1} (standard run = 3.3).
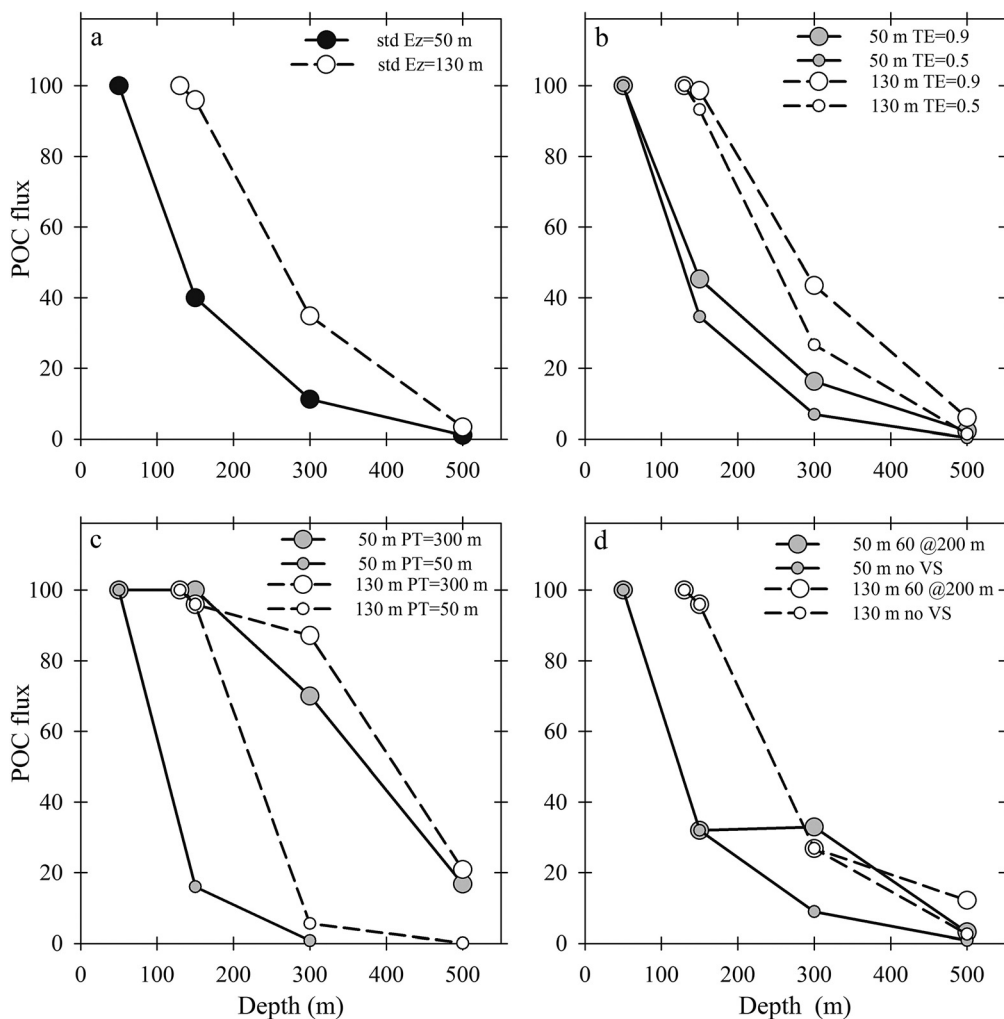
Fig. 4. Model output for a standardized POC flux of 100 mg C m^{-2} d^{-1} as predicted for 150, 300, and 500 m. (a) The standard runs are for conditions outlined in Table 2 for Ez = 50 m (filled circles) and 130 m (open circle). Sensitivity runs are then plotted for the standard runs and two euphotic-zone depths, changing one of the following: (b) the rate of bacterial solubilization, (c) the length scale of particle transformations, or (d) vertical migration as indicated on each panel and discussed in the text and Table 2.

It is clear in these sensitivity analyses that in addition to the observed changes due to varying TE, PT, and VS, different euphotic zone depths have pronounced effects on the magnitude of POC fluxes sampled at fixed depths (Fig. 4). To avoid this misinterpretation of the local particle attenuation in the twilight zone, we further explore the normalization of POC flux data to depth below Ez and thus replot flux data and model output in terms of this reference depth.

Particle flux attenuation: Flux normalized to the depth of the euphotic zone—To facilitate comparison between sites of flux attenuation normalized to depth below Ez, we also normalized all of the ^{234}Th-derived POC fluxes to a value of 1.0 at the euphotic zone. By plotting all data on a normalized basis, we can readily see the relative differences in flux attenuation at fixed distances below the base of the euphotic zone (Fig. 5). In Fig. 5, we also introduce a new metric for the transfer efficiency of fluxes below Ez. Rather than arbitrarily fit the flux data to a selected curve or

mathematical function, we have chosen to compare relative flux attenuation between sites at a reference depth 100 m below Ez, since it is in this stratum where most particle attenuation takes place and where the different sites diverge most from each other in relative POC flux (*see* dotted line in Fig. 5). We represent this difference using T_{100} as shorthand for the transfer efficiency, T_{100} = (POC flux 100 m below Ez) : (POC flux at Ez). This ratio reflects the sum of different biological processes that concurrently attenuate or increase flux in the twilight zone. The range in T_{100} is large, from 20% to ~100% (Table 5), and thus the efficiency of the biological pump differs quite significantly in the upper twilight zone between these sites.

It is interesting that there is one case, during a spring bloom in the North Atlantic, where there was no measurable flux attenuation, and so T_{100} ~100%. Of the other sites, POC flux at KIWI-8 was the least attenuated, with a T_{100} value of 80%, and many of the sites had a T_{100} value in the 50–75% range. The exceptions to this pattern were three sites with significantly lower T_{100} values in the
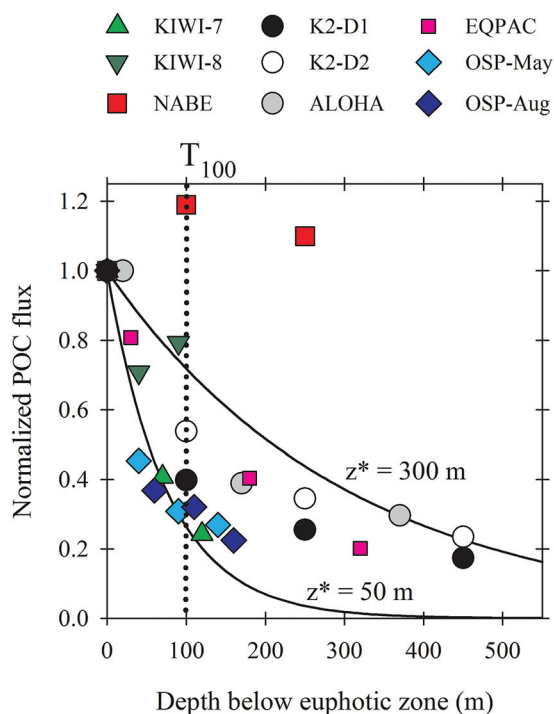
Fig. 5. Same POC flux data as in Fig. 2 and Table 1, plotted normalized to a POC flux of 1.0 at the base of the euphotic zone (*y*-axis) and relative to depth below the euphotic zone (*x*-axis). Lines for an exponential fit (Eq. 2) with a length scale of 50 m and 300 m are shown. The magnitude of shallow flux attenuation can be quantified as the transfer efficiency, T_{100} = (POC flux 100 m below Ez):(POC flux at Ez), as indicated by the dotted line at 100 m.

20–30% range, both occupations of OSP and early spring sampling in the Southern Ocean (KIWI-7).

Our approach, of introducing these new metrics to help classify different biogeochemical provinces without the need to curve-fit the flux data, can be extended to deeper depths. In this data set (Fig. 5), there appears to be an inflection in the slope of flux vs. depth pattern that is common to all of these sites below about 100–200 m below the euphotic zone. By about 300 m below Ez, the sites converge on a transfer efficiency of 20–30%. Whether the reduced variability between sites in the transfer efficiency at depth is a common feature in the oceans cannot be established here with so few data, though it is a question that can be targeted in future studies of the twilight zone. Tracers with longer half-lives than ^{234}Th and/or deeper mesopelagic traps will be required to define these deeper flux trends.

Although the parameterization of Martin et al. (1987) served well in the past to fit POC fluxes, especially at deeper depths, T_{100} precisely quantifies differences in the functioning of the biological pump in the upper twilight zone where flux attenuation changes most. Also, it does not assume a particular mathematical function for flux vs. depth, but it quantifies the relative proportion of POC flux attenuated in the first 100 m below the euphotic zone, which is a direct measure of the efficiency of the biological pump. As such, it ties in directly to the processes that

produce, attenuate, and transport POC to depth, as described by our 1-D model of twilight zone processes.

Particle flux attenuation below the euphotic zone: Model constraints—The outputs of our subsurface model are similar in profile to that of the normalized POC flux data, and they can be used to: (1) test the merits of different sampling schemes for export flux in the ocean; (2) set constraints on the extent of biological processing of particles in the twilight zone; and (3) assess the degree of model complexity that is warranted. At present, export flux in the twilight zone is sampled at fixed depths. The standard run for both Ez values (from Fig. 4), when replotted as depth below the Ez, shows the difficulties that result from trying to "retrofit" observations of POC flux (obtained from a few fixed depths) for regions with different Ez values. There is a pronounced influence of different Ez depths on apparent particle flux attenuation 100 m below Ez; T_{100} = ~60% for Ez = 130 m, and T_{100} = 40% for Ez = 50 m (Fig. 6a). Since the attenuation of POC flux is sharpest in the upper twilight zone, a low resolution of sampling at different relative depths below Ez will give the impression of less attenuation of POC flux in the upper part of the twilight zone for a site with a deeper euphotic zone.

An improved sampling scheme for export flux in the twilight zone is presented in Fig. 6b. This simulation represents the standard runs for both 50-m and 130-m Ez for particles for hypothetical POC flux sampling. In this case, we have offset the depths "sampled" in the model run by 80 m; thus, for an Ez of 50 and 130 m, the first depth "sampled" in the model is 100 and 180 m, respectively, i.e., 50 m below the local Ez, 150 and 230 m for 100 m below Ez, etc. As expected, such a standard offset in sampling depths relative to a changing Ez gives us similar POC flux profiles in our simulations and provides insights into how future sampling of the twilight zone must be carried out in order to provide unambiguous comparisons between different regions (*see* Recommendations).

In other model runs, not presented in Fig. 6, the parameterization of twilight zone processes was altered to take into account oceanic observations (i.e., more model complexity), as opposed to a simple sensitivity analysis used to look at the envelope of variability introduced by different end-member simulations (Fig. 4). Modifications include the addition of a PT immediately below a 50-m Ez (along with our standard PT = 100 m length scale at deeper depths), as reported for particle-intercepting specialist calanoid copepods in the NE subarctic Pacific (OSP) (Dagg 1993). Evidence for enhanced remineralization directly below the euphotic zone is also inferred from the presence of a remineralization layer (excess ^{234}Th) immediately below the deep chlorophyll maximum in the Sargasso Sea (Buesseler et al. 2008*a*). In another modified model run, the rate of bacterial TE was increased below 150 m (it was constant with depth in all of the runs in Fig. 6a) as reported for bacterial exoenzyme activity in the NE Atlantic (NABE site) by Hoppe et al. (1993). The addition of a shallow PT immediately below the euphotic zone results in a more rapid attenuation of export flux at
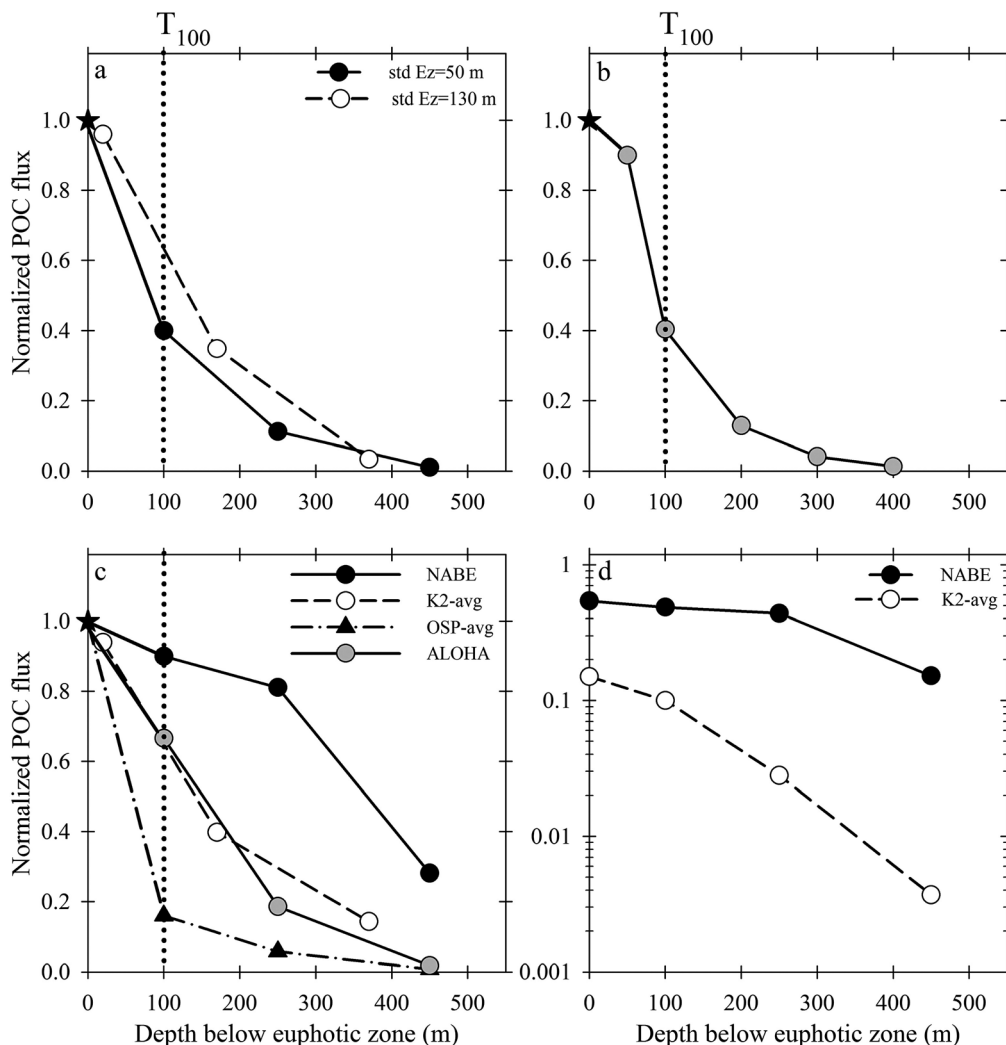
Fig. 6. Model output plotted as in Fig. 5 relative to depth below the euphotic zone and a normalized flux of 1.0 at that depth. (a) Standard runs from the model for both the 50-m and 130-m exit depths sampled in the model from "absolute depths" of 150 m, 300 m, and 500 m and replotted as depth below the euphotic zone. (b) Illustration of how a higher-resolution sampling scheme results in a better comparison of fluxes between sites with different euphotic-zone depths (*see* text for details). (c) Model runs that best approximate observed processes at four open-ocean sites, including NABE (50-m Ez, increasing TE with depth, low VS, long PT); K2 (50-m Ez, subsurface increase in TE then a decrease, high VS, PT below Ez, 150-m PT at depth); ALOHA (130-m Ez, increasing TE with depth, avg. VS, std PT), and OSP (50-m Ez, decrease in TE with depth, std VS, PT below Ez, std PT at depth). For K2 and OSP, where the observations suggest seasonal variability, the model represents average conditions for the two time periods sampled. (d) Simulation where the flux at the euphotic zone is determined by the model Ez-ratio, such that surface attenuation of NPP can be visualized by the starting point at depth (= 0.54 in NABE, 0.15 in K2) and POC attenuation in the twilight zone can be visualized by the normalized POC flux relative to this value at the euphotic zone (model parameters as in Fig. 6c), thus allowing visualization of the importance of surface vs. subsurface processes in attenuation of POC flux. Note the log scale for y-axis.

100 m below Ez (T_{100} = 16% vs. 40%, data not shown), whereas the decrease in bacterial solubilization of particles with depth slows the attenuation of export flux, as would be expected, but the absolute difference is small (flux is 2.0 vs. 1.1 mg C m^{-2} d^{-1} at 500 m for the depth-dependent bacterial TE relative to the standard run). In both cases, the shape of each profile remains broadly consistent with what is observed for export fluxes in sediment trap or ^{234}Th data sets.

The incorporation of ocean observations into the subsurface model is taken a step further in Fig. 6c, in which the twilight zone characteristics of TE, VS, and PT

for four open-ocean studies were used to provide site-specific simulations. For example, at the NABE site, there is evidence of a long PT length scale from observations of phytodetritus in deep traps (Honjo and Manganini 1993), a decrease in bacterial solubilization with depth (Hoppe et al. 1993), and little evidence of a large VS at this site in spring (Dam et al. 1993). The model (for parameter details, *see* Fig. 6 caption and Discussion) reproduces the general trends of relatively minor flux attenuation at NABE at least in the upper 300 m (T_{100} = 90%). For both K2 and ALOHA, the model, as modified to mimic twilight zone processes for these sites, predicts a similar transfer

efficiency (T_{100} = 67% and 65% for K2 and ALOHA, respectively) compared to observations (T_{100} = 47% and 67% for K2-average and ALOHA, respectively). For OSP, the model underestimates the transfer efficiency (T_{100} = 16% in model vs. 31% in observations).

The final panel (Fig. 6d) combines simulations from the surface and subsurface models (Fig. 1) to provide a simple graphic to address the relative influences of the surface vs. the subsurface ocean in attenuating the NPP signal. Here, rather than start with a normalized Ez of 1.0, we use the surface model estimate of the Ez-ratio as the flux at Ez. In the two cases chosen, model Ez-ratio = 54% for NABE and 15% for K2. Below the euphotic zone, the subsurface model uses site-specific parameters at NABE and K2 (as in Fig. 6c). For K2, the simulations indicate that although 85% of the NPP signal is attenuated in the euphotic zone (i.e., only 15% of NPP leaves Ez), there is a subsequent 40-fold decrease in the export flux by 450 m, and thus a greater effect of the subsurface than the surface ocean in setting overall POC export at depth. In contrast, at the NABE site, there is a relatively even contribution by both the euphotic-zone (NPP from 1 to 0.54) and the twilight-zone (0.54 to 0.15 by 450 m) processes in attenuating NPP (Fig. 6d).

Discussion

Our goal was to better understand the relative importance of the surface ocean (i.e., where the ''strength'' of the biological pump is set) and the subsurface ocean (i.e., where the ''efficiency'' of the biological pump is determined) in setting the magnitude of, and controls on, particle export. To accomplish this, we conducted a retrospective analysis of selected open-ocean POC flux studies and investigated a range of modeling simulations of twilight zone processes. From this, it became evident that our current approaches to both sampling the particle flux through the twilight zone (based on flux measurements at fixed depths) and the subsequent analysis of these data (curve-fitting) are both flawed. Therefore, we commence this discussion with an assessment of the new metrics that we devised to overcome the need for curve-fitting, and we evaluate how well they describe the functioning of the biological pump. Next, we devote the majority of the remainder of the discussion to testing the suitability of these metrics for characterizing regional and seasonal signatures of the biological pump and to comparing these to model predictions for four of the sites. The comparison of sites allows us to also consider whether particle mineral content and/or seasonality of export act as additional controls on the strength and efficiency of the biological pump (Armstrong et al. 2002; Francois et al. 2002; Lutz et al. 2007). Such a data comparison can be used to explore additional understanding of twilight zone processes that will potentially be achieved using this new conceptual framework. This enables us to offer a rationale and a set of recommendations for future efforts in twilight zone research.

Comparison of NPP, Ez-ratios, and T$_{100}$—We consider the ocean as a layered system, where NPP in the euphotic zone sets an upper limit on POC export flux. For each biogeochemical province, the food-web structure and physico-chemical conditions set the ratio of POC flux at the base of the euphotic zone to NPP, which we call the Ez-ratio. This metric differs from export ratios calculated for a fixed depth, since Ez varies regionally, and during the algal growth season, by <40 m to >100 m at our selected sites. To quantify flux attenuation below the euphotic zone, we use T_{100}, which is the ratio of POC flux 100 m below the euphotic zone to POC flux at the euphotic zone. We focus on the upper twilight zone where we see the greatest difference between sites and sharpest POC flux attenuation in these first 100 m, though this type of flux comparison should also be extended to greater depths.

These three metrics, NPP, Ez-ratio, and T_{100}, provide a common framework for comparing sites, and they offer an alternative to curve-fitting of flux data. We have plotted all of the metrics together (Fig. 7) to assess their ability to serve as a useful tool to tease apart differences in the twilight zone biogeochemistry between sites. They are presented as follows: the magnitude of NPP is indicated by the area of the bubble, which is plotted at the Y coordinate corresponding to the local Ez-ratio and X coordinate equal to t$_{100}$. Hence, a large circle in the upper right corner of this plot is indicative of a site with the strongest and most efficient biological pump, and maximum Ez-ratios close to 0.5 (half the NPP is exported) are consistent with the upper limit for new production suggested by Eppley and Peterson (1979). A T_{100} value of up to 1.0 would suggest no measurable flux attenuation in the upper twilight zone, which implies very low heterotrophic consumption of export flux and/or the addition of POC at depth from other sources (such as active transport by vertical migrators).

Since Ez-ratios and T_{100} both are derived from the POC flux at the euphotic zone, there is an inverse relationship between NPP and POC flux 100 m below the euphotic zone captured by the contours in Fig. 7. For example, if only 1% of NPP reaches a depth of 100 m below the euphotic zone, this may be due to a low POC flux out of the euphotic zone (low Ez-ratio) or rapid flux attenuation in the upper twilight zone (low T_{100}), or some combination thereof that would track the 1% contour line in Fig. 7. Stronger and more efficient biological pumps are characterized by higher values of both the Ez-ratio and T_{100}, i.e., moving toward the upper right of this plot (5%, 10%, 20%, 30%, and 40% contours are plotted). Some of these data represent different phases of the seasonal productivity cycle and subsequent export, and therefore this plot can also be used to capture that temporal variability (*see* K2 and KIWI case studies).

Comparison of NPP, Ez-ratios, and T$_{100}$: *Case studies*—The selected sites represent a wide range of conditions for the strength (Ez-ratio) and efficiency (T_{100}) of the biological pump and hence provide a robust test of the application of these new metrics. Moreover, our selection of sites contained both high and low extremes with respect to Ez-ratio and efficiency of export through the twilight zone, indicating that we may have captured most of the
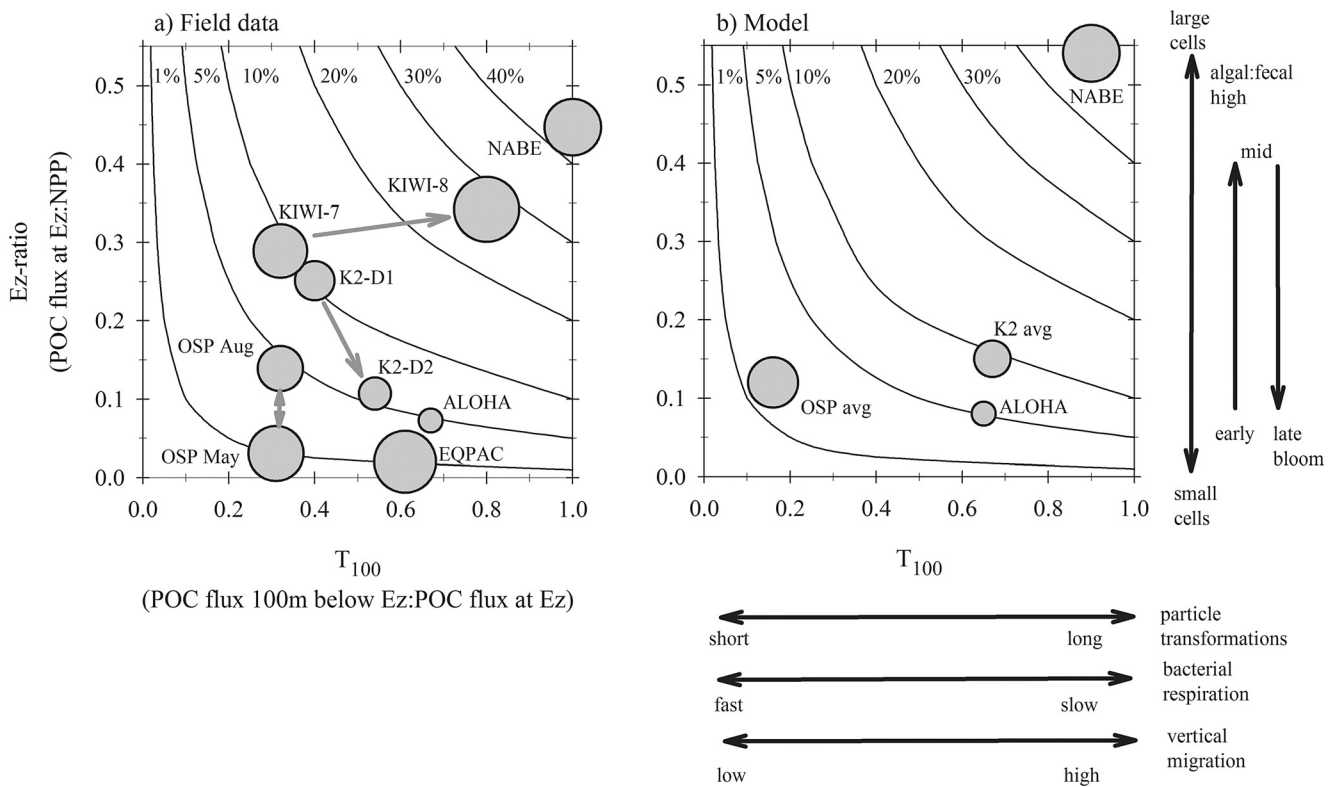
Fig. 7. Plot of Ez-ratio vs. T_{100} where the area of the circle for each site is proportional to NPP. (a) Field data from the study sites; arrows between those sites indicate temporal changes when there was repeated sampling during one field year (KIWI, OSP, K2) as discussed in the text. (b) Predictions of these same parameters using our biological model. The contour lines from 1% to 40% show the relationships between the POC flux 100 m below the euphotic zone and NPP. Also in (b), arrows along the *y*- and *x*-axes indicate the processes that would move a particular system higher or lower on these scales.

global span of such permutations for biogeochemical provinces. Interestingly, there are data points distributed across all of the contours from 1% to 40% in Fig. 7. They represent a range of conditions, from KIWI-7, which is characterized by moderately high surface export (Ez-ratios >0.3) and rapid subsurface attenuation of flux (low T_{100}), to those such as EQPAC, K2-D2, and ALOHA, where most of the attenuation of NPP is set in the surface (low Ez-ratios) and there is relatively little flux attenuation in the subsurface (high T_{100}). The range in Ez-ratios and T_{100} leads to a net flux of POC 100 m below the euphotic zone relative to NPP that varies from about 1% to >40% (Fig. 7). Combined with the variability in NPP, this represents an even wider range of POC flux at depth, from around 10 to 500 mg m^{-2} d^{-1} at 100 m below the euphotic zone (Table 5). Also, some of the data represent different phases of a seasonally changing NPP and export cycle, and they demonstrate that temporal changes in the strength and efficiency of the biological pump may be, for some sites, larger than regional differences and must be considered when comparing oceanic provinces (KIWI-7 and KIWI-8; K2-D1 and K2-D2; *see* below). We will look at each site in more detail to examine the way in which our classification scheme relates to the biogeochemical observations from each study.

The spring bloom in the North Atlantic represents an end member in our study with both high Ez-ratios (0.45)

and a T_{100} near 100%, i.e., about half of the NPP is exported out of the euphotic zone, and there is low POC flux attenuation in the first 100 m below the euphotic zone (Fig. 7a). Therefore, it represents an extremely strong and efficient biological pump (>40% NPP found 100 m below Ez). In NABE, Dam et al. (1993) found that <5% of the POC flux could be attributed to mesozooplankton fecal pellets, consistent with a high fraction of sinking algal aggregates. Given the high T_{100}, these aggregates appear to be sinking relatively unaltered through the upper twilight zone. This is supported by the 1000 m moored-trap record, which showed both high phytoplankton abundances and a large POC flux associated with bloom aggregates that was "greener and looked like plankton debris" (Honjo and Manganini 1993). We thus attribute the NABE high T_{100} to direct algal sinking with low flux attenuation, as even one transformation, through a zooplankton gut for example, would decrease T_{100} by more than a factor of two in our subsurface model.

OSP falls between the 1% and 5% contours (Fig. 7a) and thus has a low export potential for NPP (<1–5% of NPP reaches 100 m below Ez). At OSP, between May and August, the Ez-ratio varies from 0.03 to 0.14 (using POC flux data), and most of that flux is attenuated in the first 100 m of the twilight zone (T_{100} ~30%). In this case, we have too few observations to track the seasonal progression in POC flux (only one station for ^{234}Th-derived export

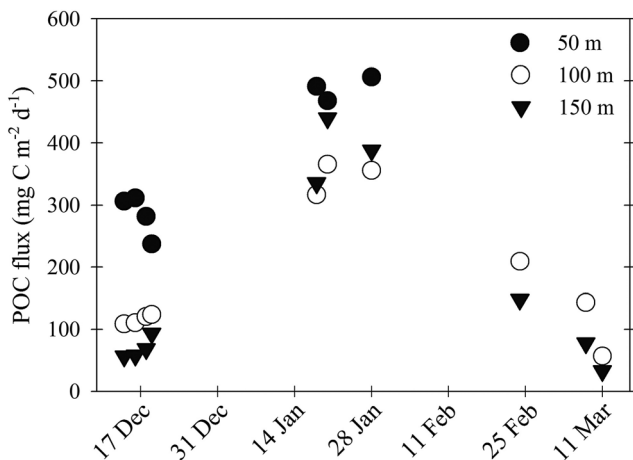Fig. 8. Seasonal cycle of POC flux (mg C m^{-2} d^{-1}) for three depths as derived from ^{234}Th data collected during the 1997 to 1998 U.S. JGOFS program south of the Polar Front along 170°W. Each set of flux estimates on a given day is from a single sampling station, with the early, mid-, and late time periods corresponding to cruise IDs KIWI-7, -8, and -9, respectively, in the U.S. JGOFS database (http://usjgofs.whoi.edu/jg/dir). There were no estimates of POC flux at 50 m during KIWI-9 given the deep mixed layer (>50 m), so the data were not used to estimate Ez-ratio or T_{100} given only two sampling depths. Note that fluxes at each station during a given cruise showed a similar seasonal pattern, with highest fluxes during January. POC flux differences between 50 m and 100 m (or 150 m) were largest during the first cruise in December.

during each season) and high variability in NPP (Boyd and Harrison 1999; Boyd et al. 1999), so we do not consider the small variability in Ez-ratios between May and August to be significant. However, on regional scales, OSP represents a system with both relatively low export fluxes and high remineralization in the upper twilight zone. This is consistent with the food web in these high-nutrient low-chlorophyll (HNLC) waters, which is dominated by phytoplankton <5 μm (Boyd and Harrison 1999) that are under tight grazer control (Landry et al. 1993). In addition, just below the euphotic zone, there is evidence of specialist particle-intercepting zooplankton (Dagg 1993). Together, this tight food-web control in the surface ocean and extensive particle transformations in the subsurface appear to drive the system to one characterized by both a weak biological pump in the surface ocean and low efficiency of the biological pump below, and thus low POC export at depth relative to modest values of NPP.

The KIWI-7 (December) and KIWI-8 (January) data are from the seasonally ice-covered region in the Pacific sector of the polar Southern Ocean. Both time periods show higher than average Ez-ratios, but transfer efficiency shifts from low (T_{100} = 30%, similar to OSP) to high (80%) within one month. Flux profiles from multiple stations (Fig. 8) confirm that the seasonal flux peak is in January, and they reveal that the differences between shallow and deep fluxes (50 m vs. 100–150 m POC flux) are greatest early in the growth season (i.e., a lower T_{100} in December). The high Ez-ratios in December and January are consistent with large diatoms dominating this ice-edge bloom (Landry

et al. 2002; Buesseler et al. 2003). As the bloom progressed, both dissolved Si and Fe decreased significantly in surface waters (Measures and Vink 2001). The onset of algal iron limitation may increase diatom frustule thickness, thereby increasing sinking rates (Hutchins and Bruland 1998; Waite and Nodder 2001). This mechanism is one way to account for the observed shift to a higher T_{100} in January. An important point is that the seasonal shift in T_{100} at this locale is as great as the regional variability in Fig. 7, so capturing and understanding this temporal variability will be important in comparing the efficiency of different biological pumps.

The remaining three sites, K2, ALOHA, and EQPAC, have a similar T_{100}, but they differ in the magnitude of NPP (lowest at ALOHA) and most significantly in the fraction of NPP that is exported below the euphotic zone (Ez-ratios from 0.25 at K2-D1 to ~0.02 for EQPAC). K2, in the northwest Pacific, was sampled ~50 d after a peak in surface phytoplankton biomass (Buesseler et al. 2008b). POC flux at 150 m decreased during deployments 1 and 2 (D1 and D2 were separated by 10 d) and at the same time the fraction of primary production attributed to large cells >20 μm decreased from 30% to 20% (Boyd et al. 2008). The Ez-ratio decreased consistent with this shift to smaller phytoplankton, yet the transfer efficiency below, T_{100}, did not change significantly. The relatively high and constant transfer efficiency despite decreasing fluxes has been noted previously from the 150- to 500-m trap data (Buesseler et al. 2007b). An in situ settling velocity sediment trap indicated that >50% of the flux sank at >100 m d^{-1} in both D1 and D2 (Trull et al. 2008), and the geochemical and biological makeup of the sinking flux did not change appreciably (Lamborg et al. 2008; Wilson et al. 2008). The rapid particle sinking velocities suggest a relatively long length scale for particle transformations for both D1 and D2. Moreover, for both D1 and D2, there was also direct transport by migrating zooplankton of a substantial fraction of the flux at depth (Steinberg et al. 2008b). Thus, a change in the strength of the biological pump in surface waters does not necessarily lead to an immediate change in the efficiency of the pump below.

ALOHA and EQPAC also have a high T_{100}, but they are among the lowest for the fraction of NPP that is exported from the euphotic zone (fraction NPP at 100 m below Ez = 1–5%). Our Ez-ratio of 7% at ALOHA from VERTIGO is the same as the long-term mean e-ratio of 7% for the Hawaii Ocean Time-series (HOT 1988–1993; Karl and Lukas 1996). We attribute the low Ez-ratio to the efficient recycling of C in the pelagic food web dominated by picophytoplankton (Buesseler et al. 2008b). As discussed previously (Fig. 2), EQPAC represents an HNLC region characterized by efficient pelagic recycling of NPP by small mesozooplankton and microzooplankton (Landry et al. 1997). Both ALOHA and EQPAC have a relatively high T_{100}, suggesting that the small fraction of POC that exits the euphotic zone is efficiently transported to depth. Perhaps because of the deeper euphotic zone at both sites, there are already multiple particle-transformation steps in the surface ocean (consistent with a low Ez-ratio) and a

longer POC residence time, such that particles are already more degraded than at sites where the euphotic zone is shallower.

Comparison of NPP, Ez-ratios, and T_{100}*: Simulations vs. observations*—In this study, there are four sites where enough information and ancillary data for the twilight zone are available to also make a comparison of the observed T_{100} values vs. those predicted from the subsurface model (K2, ALOHA, NABE, and OSP; Fig. 6c). We combined our model flux estimates in Fig. 7b, using average values for K2 and OSP, to illustrate how the model predictions can be linked to explore the relative contributions that surface and subsurface waters make to setting export flux.

The well-established surface model does a reasonable job based upon comparisons of predicted export production and the POC flux at the euphotic zone (Fig. 2 and discussion thereof). For all four sites, the model subsurface POC flux attenuation is within 50% of the value measured at these sites (predicted : measured T_{100}) l in some cases, the model underestimates the observed flux (OSP), and in others cases, the model overestimates it (K2; Table 5). Here, we explore whether the subsurface model over- or underpredictions are due to a systematic problem with the model for all sites, or to site-specific issues (as each model simulation was based on the site-specific twilight zone characteristics). To match the observations in POC flux at the NABE, our subsurface model would require essentially zero bacterial solubilization and/or higher rates of vertical migration to end up with no attenuation in POC flux as observed in the upper 100 m of the twilight zone. Zooplankton and bacterial respiration data from this site suggest that such a change to the model simulations would be unreasonable (Dam et al. 1993; Ducklow et al. 1993). Despite slight underestimation by the model, it appears that the selection of a long PT length scale mimics the direct sinking of aggregates, as observed in NABE, and this site is the most efficient biological pump in terms of both shallow export and transport below (i.e., located >40% contour in both field data and model; Fig. 7b).

For the K2 and ALOHA sites, the POC attenuation predicted by the model is higher at K2 and comparable to that observed at ALOHA during VERTIGO (predicted : measured T_{100} = 1.4 for K2 and 0.97 for ALOHA; Table 5). In VERTIGO, there were ancillary data to set the subsurface model simulations at each of these sites. For example, our site-specific model parameterization for bacterial solubilization at K2 took into account decreased bacterial solubilization directly below the euphotic zone, inferred from lower rates of bacterial production within a distinctive temperature minimum layer between 50- and 100-m depth (B. Van Mooy pers. comm.; Table 5). Furthermore, for K2, we chose to parameterize the model with an initial PT immediately below the euphotic zone, given the shallow euphotic zone and some evidence from [234]Th and nutrient budgets of significant remineralization between 50 and 150 m (Buesseler et al. 2008b; in press; Elskens et al. 2008). At depths below this initial PT, we used a longer PT length scale (150 m) due to the larger size of zooplankton fecal pellets at K2 relative to ALOHA,

which, along with their higher mineral content, would increase sinking rates (Buesseler et al. 2007b; Wilson et al. 2008). Zooplankton net tows showed significant diel migration to the 0–50-m stratum and, to a lesser extent, the 50–100-m layer immediately below the euphotic zone, equivalent to 70% of the POC flux at 150 m (Steinberg et al. 2008a). This activity was represented by a vertical shunt of 70 mg C m^{-2} d^{-1} POC to 100 m below the euphotic zone in the model. Still there are uncertainties as to how much carbon to shunt and to what depth, but this active transport pathway was certainly larger than at ALOHA.

At ALOHA, our site-specific model parameterization included a slight decrease in bacterial solubilization below 150 m based upon observations of bacterial production vs. depth (Table 5; TE dropped from 0.6 to 0.7). Observations from thorium and from mesozooplankton distributions (Steinberg et al. 2008a; Buesseler et al. in press) did not indicate the presence of high remineralization or zooplankton activity just below the euphotic zone, and hence we did not parameterize the model with an initial PT directly below the euphotic zone, and instead we used the standard PT length scale of 100 m below. Also, zooplankton transport by diel migrants was observed to be equivalent to 30% of the POC flux at 150 m (Steinberg et al. 2008a), and thus a VS of 30 mg C m^{-2} d^{-1} was used.

At OSP, the predicted POC flux at T_{100} was significantly lower (predicted : measured = 0.5; Table 5) than values observed in either May or August. There are some difficulties in trying to predict export flux using a single model simulation for two different months. In May, OSP is characterized by zooplankton transforming particles immediately below the euphotic zone (Dagg 1993) and low diel vertical migration (Goldblatt et al. 1999). Significantly, in August at OSP, the ontogenetic migration to depth of the neocalanoid copepods has taken place, and there is evidence of more diel vertical migration, compared to May, by relatively small copepods (Goldblatt et al. 1999). However, the ratios of the observed POC flux at the euphotic zone to 100 m below are very similar in both months (Table 5), suggesting that other particle-transformation processes must be important. We would expect the model, as it was parameterized, to provide a better estimate of the observed flux in May and underestimate the flux in August (since, in both cases, it was run with an initial PT immediately below the mixed layer). However, the model underestimates the flux in both months, suggesting that other observations are required to provide insights into how the model parameterization can be used to better represent twilight zone processes at this site.

When both the surface and subsurface models are linked, the cumulative simulations predict that each site would fit into roughly similar contour lines in Fig. 7b, as seen in the data (Fig. 7a), and the fraction of NPP reaching 100 m below the euphotic zone would follow the order NABE > K2 > ALOHA > OSP. Therefore, to first order, the model captures the range in biological pump differences, and it also offers some insights into how different particle-transformation processes alter POC flux through the water column (*see* arrows in Fig. 7b along *x*- and *y*-axes).

While our subsurface model may need to become more complex, the model sensitivity analysis already enables us to rule out several scenarios as being unrealistic, since they have not been observed at sites across a wide range of biogeochemical provinces. For example, the shortest PT length scale resulted in POC fluxes that markedly underestimate observed POC fluxes and the envelope of data (based on a range of sites) that they represent (Fig. 4c). This suggests that a PT length scale of 50 m or less is unlikely to exist or persist in any region over the upper 500 m of the water column. In contrast, length scales longer than 300 m for PT overestimate the observed POC flux but are relatively similar to end members from the observations of direct algal settling. Thus, we can constrain PT length scales as being >50 m and <300 m across a wide range of oceanic settings.

The PT length scales can be related to observed sinking rate data, either directly (in situ settling column sediment traps; Peterson et al. 2005; Trull et al. 2008, R. A. Armstrong unpubl.) or indirectly (peak matching of trap pulses; Honjo and Manganini 1993; Berelson 2002); thus, these PT length scales correspond to <1–3 d transit times for particles settling through the water column at sinking rates of >100–350 m d^{-1} (based upon a 300-m transit below the euphotic zone). This suggests that sinking particles passing through the upper twilight zone are intercepted perhaps once or twice per day by grazers and detritivores.

We also found that it was difficult for our model to produce an increase in flux at depth, unless the vertical shunt transported 38% or more of the POC exiting the euphotic zone to depths greater than 200 m. While the range in field estimates for the importance of active transport by zooplankton relative to direct sinking of POC export spans <10% to 100% (Longhurst et al. 1990; Steinberg et al. 2000, 2008a), the lack of subsurface maxima in most POC flux profiles suggests that the average VS must be <40% of POC export, or we would expect to see a greater number of sites characterized by increasing POC flux at depth.

Can we improve the subsurface model?—While our model can be criticized as being overly simplistic, it does reproduce a range of settings, including those where particle attenuation is controlled primarily by surface processes (low Ez-ratios) or subsurface remineralization (low T_{100}). Bacterial solubilization seems least sensitive to changes in the way its influence on POC export fluxes is parameterized (Fig. 4b). Depth dependency of the terms used in the model—such as the VS or PT—may improve the model representation of twilight zone processes, but we have insufficient data to justify a more complicated model at present. There may be additional processes that should be included (*see* the OSP case above), such as faunistics (e.g., salps vs. copepods), algal aggregates formed by different stickiness factors, and/or seasonal vs. diel zooplankton migration. However, much of this can presently be mimicked by appropriate parameter choices in this simple model, such as using longer PT length scales for fast-sinking salp pellets or direct algal settling, and

variable or multiple depths for VS, etc. With so few data and our limited understanding of biological processes in the twilight zone, for now we also chose not to fine-tune the model to fit the data or use higher vertical resolution in the model than is typically observed in the field data.

However, even these simple model simulations provide insights into which data sets from future studies of the twilight zone would enable improved validation or parameterization of the model. Clearly, data are needed to help us test whether the PT length scale approach requires fine-tuning (such as depth dependency). Vertically resolved data would be useful regarding the trophic mode, vertical movement, activity, and abundance of a range of zooplankton groups and species throughout the twilight zone. For example, there is now initial evidence of depth-dependent changes in the composition of fecal pellets that reflect different trophic modes and distinct layers of zooplankton that produce new pellets de-novo either by feeding on suspended or sinking POC, or each other (Wilson et al. 2008). If this carnivory at depth is dependent upon diel migrators that feed in surface waters, then this process in effect becomes an additional VS term that needs to be included in our model. Similarly, more information to improve the parameterization of bacterial solubilization of sinking particles would be useful, such as on depth-dependent changes in growth efficiency and the fraction of attached vs. free-living bacteria.

Reinterpretation of the K2 and ALOHA data sets from VERTIGO—These data show similar, or even slightly less, subsurface flux attenuation for ALOHA (T_{100}= 67%) relative to K2 (T_{100}= 40–54%), despite large differences in the local surface food-web structure and particle sources. This may seem at odds with our previously published K2 and ALOHA flux data, which we interpreted as showing higher flux attenuation at ALOHA between 150 m and 500 m for traps at the same fixed depths (Buesseler et al. 2007b). Using the Martin curve fit to these data, the larger negative *b* value for ALOHA vs. K2 supports this more traditional view (Table 6). However, we also noted the difference in euphotic zone between sites (Buesseler et al. 2007b, 2008b) as one factor to consider when sampling flux at different relative depths below the euphotic zone. So, the conclusion here of a comparable T_{100} between these sites is based upon POC flux estimates from ^{234}Th at depths <150 m for K2, a depth horizon not directly sampled with sediment traps during VERTIGO. In an absolute sense, the biological pump at K2 still transports more POC flux to depth (POC flux 100 m below Ez = 68 and 25 mg m^{-2} d^{-1} for K2-D1 and K2-D2, respectively, vs. 10 mg m^{-2} d^{-1} for ALOHA; Table 5), but the difference in relative flux attenuation below the euphotic zone is not as large as the Martin curve-fitting procedure had suggested. This illustrates, in part, the difficulty in fitting flux vs. depth patterns using a Martin curve as the diagnostic for remineralization. It also points out that different biological processes can lead to the same T_{100}, so better identification and parameterization of different biological processes that affect flux below the euphotic zone will be important in the future.

Other controls on particle export and remineralization in the twilight zone—We have proposed a new conceptual framework to better capture flux differences between sites that can then be related to the mechanisms controlling the magnitude and efficiency of particle export. We will now use this framework to briefly examine two recent hypotheses regarding particle flux attenuation, namely, ballast controls and the role of seasonality (i.e., blooms).

There has been considerable discussion on the geochemical correlation between deep-trap fluxes and $CaCO_3$ content of settling particles, the so-called ballast hypothesis (Armstrong et al. 2002). Using regional differences in deep-ocean fluxes and correlations with mineral content, it was suggested that ballasting, in particular, by $CaCO_3$ minerals, "promotes export of organic carbon to the deep sea" (Francois et al. 2002), either by increasing specific gravity and hence sinking rates, or by protection of POC from microbial degradation (Hedges et al. 2001; Armstrong et al. 2002; Francois et al. 2002). While these correlations hold for deep-trap records, there are few data in the twilight zone to support this, i.e., no correlations of sinking rate vs. mineral content in the twilight zone (C. Lee unpubl.; Trull et al. 2008) and, likewise, no correlation between seasonal changes in deep-ocean POC flux and $CaCO_3$ content, which would be expected if the mechanism for enhanced POC flux were a direct result of changing mineral content (Boyd and Trull 2007). There are also data suggesting that the mineral : POC correlation is a function of sorption properties for organic matter, so mineral content may be a response to changes in POC flux rather than a cause of flux changes (Passow and De La Rocha 2006).

We find that by placing data from our selected sites in the framework of our new flux metrics, two sites with a higher $CaCO_3$ content for sinking particles do have relatively high transfer efficiency, namely ALOHA and EQPAC, but they do not necessarily export a high fraction of NPP out of the surface ocean (i.e., T_{100} is high and Ez-ratio is low). However, sites with high biogenic Si content for sinking particles can also have a high T_{100} (KIWI-8 and K2-D2). In addition, NABE had the strongest and most efficient biological pump driven by direct settling of diatoms (Fig. 7). So in this twilight zone data set, the calcium carbonate content of sinking particles is not the only factor that determines when or where the overall efficiency of the biological pump can be high.

Since many of the highest export events are seasonal, as evidenced, for example, in deep-ocean-trap time-series (Deuser 1986), the episodic nature of export flux and temporal changes among NPP, export, and flux attenuation need to be considered. Our new metrics for characterizing the biological pump can be used to capture some of that dynamic. Also, as mentioned previously, with particle sinking rates >100–350 m d^{-1}, this implies that the flux profile would be rapidly reset within a few days if the quantity or composition of sinking matter were to change in the surface ocean, so time-series sampling through one of these shifts in export efficiency would be informative.

Our most efficient biological pump was associated with the spring diatom bloom in the North Atlantic, in terms of the fraction of NPP that exits the euphotic zone and that survives transport through the twilight zone (>40% of NPP at 100 m below Ez). At our Southern Ocean site, we observed a temporal change in the functioning of the biological pump when it went from low to high T_{100} within one month during a diatom bloom (KIWI-7 to KIWI-8; Fig. 7a). That same region, sampled in a different year (and by a different method- POC stocks, not POC fluxes) was characterized as a low-export-efficiency site—a so-called "high biomass, low export" regime—during a mesoscale in situ iron-fertilization experiment (Lam and Bishop 2007). However, the end of that iron-fertilized diatom bloom was not sampled, and low-iron conditions in these waters may be the trigger that causes increased sinking rates and high export efficiency as mentioned previously for KIWI-8. Again, samples during one season will not be representative of the region as a whole with respect to the balance between NPP and POC fluxes.

In contrast to the two blooms we sampled in the surface ocean and in the upper twilight zone, a recent data compilation of deep-moored trap fluxes suggests lower export efficiency associated with blooms (Lutz et al. 2007). However, evidence to support this finding is confounded by the difficulty in comparing highly variable deep-trap flux records with the long-term average primary production cycle (7 yr average NPP derived from remote sensing), which likely contributes to a mismatch in NPP and POC fluxes in some data sets. Also, some of the higher fluxes associated with blooms were obtained from moored conical traps in shallow waters where the trap collection efficiency may be low (Scholten et al. 2001; Yu et al. 2001). Finally, it is always difficult to link surface processes and deep-ocean particle flux data in a 1-D manner due to the statistical sampling of particle source funnels (Siegel and Deuser 1997; Nodder et al. 2005).

While there are some twilight zone data that indicate lower export efficiency during blooms using traditional drifting traps (Pommier et al. 2008), the longer-term time-series trap record at BATS shows no such relationship (Steinberg et al. 2001). Clearly, we do not yet have a single explanation for the reason why some studies suggest higher, lower, or no change in the biological pump efficiency following blooms, but we propose that sampling of flux relative to changing euphotic zone and the use of our new metrics (e.g., Fig. 7) will allow us to capture and compare these seasonal trends, which are at least as large as the regional differences.

Recommendations for the future

This assessment of observations and model simulations offers several important lessons for future twilight zone studies. The first step is to normalize fluxes to the depth of the euphotic zone—a departure from conventional sampling at fixed depths. Such a shift in sampling protocol would require discussion across the international community regarding the best definition of euphotic zone and designing sampling techniques to consider regional, seasonal, and daily changes in the euphotic zone.

Second, our findings suggest that the fitting of shallow flux data with a Martin power-law curve or other function

may obscure or confound interpretation of twilight zone processes. We propose three metrics, NPP, Ez ratios, and T_{100} to capture regional and seasonal differences in surface export and flux attenuation. Together, these metrics define regions of high and low surface export and subsurface flux attenuation. Comparisons of these differences will help in better understanding the underlying mechanisms that control the magnitude and efficiency of the biological pump.

We have been able to model both the fraction of NPP that leaves the euphotic zone and extend a simple 1-D model into the upper twilight zone. The subsurface model includes parameterization of POC flux attenuation by bacteria and zooplankton and active transport of POC to depth by migrating zooplankton. Taken together, the surface and subsurface models capture the wide range of modes in which the biological pump functions, as evidenced by the few sites where we have ancillary data on surface food webs and subsurface heterotrophic communities. This model framework provides insights into the type of data sets that are needed in future twilight zone studies. Ultimately, these will improve parameterization and validation of the model. Such data sets will rely upon a combination of new tools to measure key rates, such as particle flux (NBSTs, swimmer avoidance traps), in situ respiration rates associated with particle breakdown (P.W. Boyd unpubl.), and particle sinking rates, complemented by higher-resolution assessment of particle characteristics and abundances using cameras, sensors on profiling floats, and gliders.

The challenge ahead is to populate the surface ocean and twilight zone with more combined studies of geochemical properties and biological processes associated with the ocean's particle cycle. While existing data and other studies show regional and seasonal variability in the strength and efficiency of the biological pump, we are far from having predictive capabilities to model POC flux attenuation in the present-day or future ocean. Since 10×10^{12} kg C yr^{-1} is thought to be leaving the surface ocean via the biological pump (Falkowski et al. 1998), and only ~10% of that flux survives transport through the twilight zone (Martin et al. 1987), understanding of this large and variable flux is critical if we are to determine the open ocean's role in the global C cycle and climate.

References

AGASSIZ, A. 1888. Three cruises of the United States Coast and Geodetic Survey steamer *Blake* in the Gulf of Mexico, in the Caribbean Sea, and along the Atlantic coast of the United States from 1877 to 1880. Bull. Museum Comp. Zool. Harvard **1:** 1–314.

ARMSTRONG, R. A., C. LEE, J. I. HEDGES, S. HONJO, AND S. G. WAKEHAM. 2002. A new, mechanistic model for organic carbon fluxes in the ocean based on the quantitative association of POC with ballast minerals. Deep-Sea Res. II **49:** 219–236.

BACON, M. P., J. K. COCHRAN, D. HIRSCHBERG, T. R. HAMMAR, AND A. P. FLEER. 1996. Export flux of carbon at the equator during the EqPac time-series cruises estimated from ^{234}Th measurements. Deep-Sea Res. II **43:** 1133–1154.

BENITEZ-NELSON, C. R., AND W. S. MOORE. 2006. Future applications of ^{234}Th in aquatic ecosystems. A preface to a special volume of *Marine Chemistry*. Mar. Chem. **100:** 163–165.

BERELSON, W. M. 2002. Particle settling rates increase with depth in the ocean. Deep-Sea Res. II **49:** 237–251.

BERGER, W. H. 1971. Sedimentation of planktonic foraminifera. Marine Geology **11:** 325–388.

———, K. FISCHER, C. LAI, AND G. WU. 1988. Ocean carbon flux: Global maps of primary production and export production, p. 131–176. *In* C. R. Agegian [ed.], Biogeochemical cycling and fluxes between the deep euphotic zone and other oceanic realms. National Undersea Research Program Research Report 88–1. NOAA.

———, V. S. SMETACEK, AND G. WEFER. 1989. Ocean productivity and paleoproductivity—an overview, p. 1–34. *In* W. H. Berger, V. Smetacek and G. Wefer [eds.], Productivity of the ocean: Present and past: Dahlem Workshop Reports. Wiley.

BISHOP, J. 1989. Regional extremes in particulate matter composition and flux: Effects on the chemistry of the ocean interior, p. 117–138. *In* W. H. Berger, V. S. Smetacek and G. Wefer [eds.], Productivity of the ocean: Present and past. Wiley.

BOYD, P. W., M. P. GALL, M. W. SILVER, S. L. COALE, R. R. BIDIGARE, AND J. L. K. BISHOP. 2008. Quantifying the surface-subsurface biogeochemical coupling during the VERTIGO ALOHA and K2 studies. Deep-Sea Res. II **55:** 1578–1593.

———, AND P. J. HARRISON. 1999. Phytoplankton dynamics in the NE subarctic Pacific. Deep-Sea Res. II **46:** 2405–2432.

———, AND P. NEWTON. 1995. Evidence of the potential influence of planktonic community structure on the interannual variability of particulate organic carbon flux. Deep-Sea Res. I **42:** 619–639.

———, AND P. P. NEWTON. 1999. Does planktonic community structure determine downward particulate organic carbon flux in different oceanic provinces. Deep-Sea Res. I **46:** 63–91.

———, AND T. TRULL. 2007. Understanding the export of marine biogenic particles: Is there consensus? Prog. Oceanogr. **72:** 276–312.

———, AND OTHERS. 1999. Transformations of biogenic particulates from the pelagic to the deep ocean realm. Deep-Sea Res. II **46:** 2761–2792.

BUESSELER, K. O., J. A. ANDREWS, M. C. HARTMAN, R. BELASTOCK, AND F. CHAI. 1995. Regional estimates of the export flux of particulate organic carbon derived from thorium-234 during the JGOFS EQPAC program. Deep-Sea Res. II **42:** 777–804.

———, M. P. Bacon, J. K. Cochran, and H. D. Livingston. 1992. Carbon and nitrogen export during the JGOFS North Atlantic Bloom Experiment estimated from ^{234}Th: ^{238}U disequilibria. Deep-Sea Res. I **39:** 1115–1137.

———, L. Ball, J. Andrews, C. Benitez-Nelson, R. Belastock, F. Chai, and Y. Chao. 1998. Upper ocean export of particulate organic carbon in the Arabian Sea derived from thorium-234. Deep-Sea Res. II **45:** 2461–2487.

———, R. T. Barber, M.-L. Dickson, M. R. Hiscock, J. K. Moore, and R. Sambrotto. 2003. The effect of marginal ice-edge dynamics on production and export in the Southern Ocean along 170°W. Deep-Sea Res. II **50:** 579–603.

———, and others. 2006. An assessment of particulate organic carbon to thorium-234 ratios in the ocean and their impact on the application of ^{234}Th as a POC flux proxy. Mar. Chem. **100:** 213–233.

———, and ———. 2007*a*. An assessment of the use of sediment traps for estimating upper ocean particle fluxes. J. Mar. Res. **65:** 345–416.

———, and ———. 2007*b*. Revisiting carbon flux through the ocean's twilight zone. Science **316:** 567–570.

———, and ———. 2008*a*. Particle fluxes associated with mesoscale eddies in the Sargasso Sea. Deep-Sea Res. II **55:** 1426–1444.

———, and ———. 2008*b*. VERTIGO (VERtical Transport In the Global Ocean): A study of particle sources and flux attenuation in the North Pacific. Deep-Sea Res. II **55:** 1522–1539.

———, S. Pike, K. Maiti, C. H. Lamborg, D. A. Siegel, and T. W. Trull. In press. Thorium-234 as a tracer of spatial, temporal and vertical variability in particle flux in the North Pacific. Deep-Sea Research I.

Charette, M. A., S. B. Moran, and J. K. B. Bishop. 1999. ^{234}Th as a tracer of particulate organic carbon export in the subarctic Northeast Pacific Ocean. Deep-Sea Res. II **46,** (11–12), 2833–2861.

Dagg, M. 1993. Grazing by the copepod community does not control phytoplankton production in the subarctic Pacific Ocean. Prog. Oceanogr. **32:** 163–183.

Dam, H. G., C. A. Miller, and S. H. Jonasdottir. 1993. The trophic role of mesozooplankton at 47 N, 20 W during the North Atlantic Bloom Experiment. Deep-Sea Res. II **40:** 197–212.

Deuser, W. G. 1986. Seasonal and interannual variations in deep-water particle fluxes in the Sargasso Sea and their relation to surface hydrography. Deep-Sea Res. **33:** 225–246.

Ducklow, H. W., D. L. Kirchman, H. L. Quinby, C. A. Carlson, and H. G. Dam. 1993. Stocks and dynamics of bacterioplankton carbon during the spring bloom in the eastern North Atlantic Ocean. Deep Sea Res. II **40:** 245–263.

Dunne, J. P., R. A. Armstrong, A. Gnanadesikan, and J. L. Sarmiento. 2005. Empirical and mechanistic models for the particle export ratio. Glob. Biogeochem. Cy. **19:** GB4026, doi:10.1029/2004GB002390.

Elskens, M., W. Baeyens, P. Boyd, K. Buesseler, F. Dehairs, N. Savoye, and B. Van Mooy. 2008. Primary, new and export production in the NW Pacific Subarctic Gyre during the VERTIGO K2 experiments. Deep-Sea Res. II **55:** 1594–1604.

Eppley, R. W. 1989. New production: History, methods, problems, p. 85–97. *In* W. H. Berger, V. S. Smetacek and G. Wefer [eds.], Productivity of the ocean: Present and past. Wiley.

———, and B. J. Peterson. 1979. Particulate organic matter flux and planktonic new production in the deep ocean. Nature **282:** 677–680.

Falkowski, P. G., R. T. Barber, and V. Smetacek. 1998. Biogeochemical controls and feedbacks on ocean primary production. Science **281:** 200–206.

Fasham, M. J. R. 2003. Ocean biogeochemistry: The role of the ocean carbon cycle in global change. Springer.

Francois, R., S. Honjo, R. Krishfield, and S. Manganini. 2002. Factors controlling the flux of organic carbon to the bathypelagic zone of the ocean. Glob. Biogeochem. Cy. **16:** 1087.

Gardner, W. D. 2000. Sediment trap technology and sampling in surface waters, p. 240–281. *In* R. B. Hanson, H. W. Ducklow and J. G. Field [eds.], The changing ocean carbon cycle: A midterm synthesis of the Joint Global Ocean Flux Study. Cambridge Univ. Press.

Goldblatt, R. H., D. L. Mackas, and A. G. Lewis. 1999. Mesozooplankton community characteristics in the NE subarctic Pacific. Deep-Sea Res. II **46:** 2645–2668.

Hedges, J. I., J. A. Baldock, Y. Gelinas, C. Lee, M. Peterson, and S. G. Wakeham. 2001. Evidence for non-selective preservation of organic matter in sinking marine particles. Nature **409:** 801–804.

Honda, M. C., H. Kawakama, K. Sasaoka, S. Watanabe, and T. Dickey. 2006. Quick transport of primary produced organic carbon in the ocean interior. Geophys. Res. Lett. **33:** L16603, doi:10.1029/2006GL026466.

Honjo, S. 1976. Coccoliths: Primary production, transportation and sedimentation. Mar. Micropaleont. **1:** 65–79.

———, R. Francois, S. Manganini, J. Dymond, and R. Collier. 2000. Export fluxes in the western Pacific sector of the Southern Ocean along 170°W. Deep-Sea Res. II **47:** 3521–3548.

———, and S. J. Manganini. 1993. Annual biogenic particle fluxes to the interior of the North Atlantic Ocean; studies at 34°N 21°W and 48°N 21°W. Deep-Sea Res. II **40:** 587–607.

———, ———, R. A. Krishfield, and R. Francois. 2008. Particulate organic carbon fluxes to the ocean interior and factors controlling the biological pump: A synthesis of global sediment trap programs since 1983. Prog. Oceanogr. **76:** 217–285.

Hoppe, H.-G., H. W. Ducklow, and B. Karrasch. 1993. Evidence for dependency of bacterial growth on enzymatic hydrolysis of particulate organic matter in the mesopelagic ocean. Mar. Ecol. Prog. Ser. **93:** 277–283.

Hutchins, D. A., and K. W. Bruland. 1998. Iron-limited diatom growth and Si:hairsp;N uptake ratios in a coastal upwelling regime. Nature **393:** 561–564.

Jerlov, N. G. 1968. Optical oceanography. Elsevier.

Karl, D. M., and R. Lukas. 1996. The Hawaii Ocean Time-series (HOT) Program: Background, rationale and field implementation. Deep-Sea Res. II **43:** 129–156.

Kemp, P. F. 1993. Handbook of methods in aquatic microbial ecology. CRC Press.

Klaas, C., and D. E. Archer. 2002. Association of sinking organic matter with various types of mineral ballast in the deep sea: Implications for the rain ratio. Glob. Biogeochem. Cy. **16:** 1116, doi:10.1029/2001GB001765.

Knap, A. H., and others. 1997. BATS methods manual. U.S. JGOFS Planning Office.

Lam, P. J., and J. K. B. Bishop. 2007. High biomass, low export regimes in the Southern Ocean. Deep-Sea Res. Part II **54:** 601–638.

Lamborg, C. H., and others. 2008. The flux of bio- and lithogenic material associated with sinking particles in the mesopelagic "twilight zone" of the northwest and north central Pacific Ocean. Deep-Sea Res. II **55:** 1540–1563.

LAMPITT, R. S., AND OTHERS. 2008. Particle export from the euphotic zone: Estimates using a novel drifting sediment trap, [234]Th and new production. Deep-Sea Res. I **55:** 1484–1502.

LANDRY, M. R., B. C. MONGER, AND K. E. SELPH. 1993. Time-dependency of microzooplankton grazing and phytoplankton growth in the subarctic Pacific. Prog. Oceanogr. **32:** 205–222.

———, AND OTHERS. 1997. Iron and grazing constraints on primary production in the central equatorial Pacific: An EqPac synthesis. Limnol. Oceanogr. **42:** 405–418.

———, AND OTHERS. 2002. Seasonal dynamics of phytoplankton in the Antarctic Polar Front region at 170°W. Deep-Sea Res. II **49:** 1843–1865.

LONGHURST, A. R., A. W. BEDO, W. G. HARRISON, E. J. H. HEAD, AND D. D. SAMEOTO. 1990. Vertical flux of respiratory carbon by oceanic diel migrant biota. Deep-Sea Res. **37:** 685–694.

LUTZ, M., R. DUNBAR, AND K. CALDEIRA. 2002. Regional variability in the vertical flux of particulate organic carbon in the ocean interior. Glob. Biogeochem. Cy. **16:** 1037, doi:10.1029/2000GB001383.

LUTZ, M. J., K. CALDEIRA, R. B. DUNBAR, AND M. J. BEHRENFELD. 2007. Seasonal rhythms of net primary production and particulate organic carbon flux to depth describe the efficiency of biological pump in the global ocean. J. Geophys. Res. **112:** C10011, doi:10.1029/2006JC002706.

MARTIN, J. H., G. A. KNAUER, D. M. KARL, AND W. W. BROENKOW. 1987. VERTEX: Carbon cycling in the northeast Pacific. Deep-Sea Res. **34:** 267–285.

———, S. E. FITZWATER, R. M. GORDON, S. N. HUNTER, AND S. J. TANNER. 1993. Iron, primary production and carbon-nitrogen flux studies during His JGOFS North Atlantic Bloom Experiment. Deep-Sea Research II. **40:** 115–134.

MEASURES, C. I., AND S. VINK. 2001. Dissolved Fe in the upper waters of the Pacific sector of the Southern Ocean. Deep-Sea Res. II **48:** 3913–3941.

MICHAELS, A. F., AND M. W. SILVER. 1988. Primary production, sinking fluxes and the microbial food web. Deep-Sea Res. **35:** 473–490.

MURRAY, J. W., J. N. DOWNS, S. STROM, C.-L. WEI, AND H. W. JANNASCH. 1989. Nutrient assimilation, export production and [234]Th scavenging in the eastern equatorial Pacific. Deep-Sea Res. **36:** 1471–1489.

NELSON, D. M., AND OTHERS. 2002. Vertical budgets for organic carbon and biogenic silica in the Pacific sector of the Southern Ocean, 1996–1998. Deep-Sea Res. II **49:** 1645–1674.

NODDER, S. D., P. W. BOYD, S. M. CHISWELL, M. H. PINKERTON, J. M. BRADFORD-GRIEVE, AND M. J. N. GREIG. 2005. Temporal coupling between surface and deep ocean biogeochemical processes in contrasting subtropical and subantarctic water masses, southwest Pacific Ocean. J. Geophys. Res. **110:** C12017, doi:10.1029/2004JC002833.

PACE, M. L., G. A. KNAUER, D. M. KARL, AND J. H. MARTIN. 1987. Primary production, new production and vertical flux in the eastern Pacific Ocean. Nature **325:** 803–804.

PASSOW, U., AND C. L. DE LA ROCHA. 2006. Accumulation of mineral ballast on organic aggregates. Glob. Biogeochem. Cy. **20:** GB1013, doi:10.1029/2005GB002579.

PEINERT, R., B. VON BODUNGEN, AND V. S. SMETACEK. 1989. Food web structure and loss rate, p. 35–48. *In* W. H. Berger, V. S. Smetacek and G. Wefer [eds.], Productivity of the ocean: Present and past. Wiley.

PETERSON, M. L., S. G. WAKEHAM, C. LEE, M. A. ASKEA, AND J.-C. MIQUEL. 2005. Novel techniques for collection of sinking particles in the ocean and determining their settling rates. Limnol. Oceanogr. Meth. **3:** 520–532.

PLOUG, H. 2001. Small-scale oxygen fluxes and remineralization in sinking aggregates. Limnol. Oceanogr. **46:** 1624–1631.

———, AND H.-P. GROSSART. 1999. Bacterial production and respiration in aggregates – a matter of the incubation method. Aquatic Microbial Ecology **20:** 21–29.

POMMIER, J., C. MICHEL, AND M. GOSSELIN. 2008. Particulate organic carbon export in the upper twilight zone during the decline of the spring bloom. Mar. Ecol. Prog. Ser. **356:** 81–92.

PRIMEAU, F. 2006. On the variability of the exponent in the power law depth dependence of POC flux estimated from sediment traps. Deep-Sea Res. I **53:** 1335–1343.

ROBISON, B. H., K. R. REISENBICHLER, AND R. E. SHERLOCK. 2005. Giant larvacean houses: Rapid carbon transport to the deep sea floor. Science **308:** 1609–1611.

RUSSELL, F. S. 1931. The vertical distribution of marine macroplankton. X. Notes on the behaviour of Sagitta in the Plymouth area. J. Mar. Biol. Assoc. UK **17:** 391–414.

RUTGERS VAN DER LOEFF, M., AND OTHERS. 2006. A review of present techniques and methodological advances in analyzing [234]Th in aquatic systems. Mar. Chem. **100:** 190–212.

SANTSCHI, P. H., AND OTHERS. 2006. Thorium speciation in seawater. Mar. Chem. **100:** 250–268.

SAVOYE, N., AND OTHERS. 2006. [234]Th sorption and export models in the water column: A review. Mar. Chem. **100:** 234–249.

SCHOLTEN, J. C., AND OTHERS. 2001. Trapping efficiencies of sediment traps from the deep eastern North Atlantic: The [230]Th calibration. Deep-Sea Res. II **48:** 2383–2408.

SHERRY, N. D., P. W. BOYD, K. SUGIMOTO, AND P. J. HARRISON. 1999. Seasonal and spatial patterns of heterotrophic bacterial production, respiration, and biomass in the subarctic NE Pacific. Deep-Sea Research II **46:** 2557–2578.

SIEGEL, D. A., AND W. G. DEUSER. 1997. Trajectories of sinking particles in the Sargasso Sea: Modeling of statistical funnels above deep-ocean sediment traps. Deep-Sea Res. I **44:** 1519–1541.

SOUTAR, A., S. A. KLING, P. A. CRILL, E. DUFFRIN, AND K. W. BRULAND. 1977. Monitoring the marine environment through sedimentation. Nature **266:** 136–139.

STEINBERG, D. K., C. A. CARLSON, N. R. BATES, S. A. GOLD-THWAIT, L. P. MADIN, AND A. F. MICHAELS. 2000. Zooplankton vertical migration and the active transport of dissolved organic and inorganic carbon in the Sargasso Sea. Deep-Sea Res. I **47:** 137–158.

———, ———, ———, R. J. JOHNSON, A. F. MICHAELS, AND A. H. KNAP. 2001. Overview of the US JGOFS Bermuda Atlantic Time-series Study (BATS): A decade-scale look at ocean biology and biogeochemistry. Deep-Sea Res. II **48:** 1405–1448.

———, J. S. COPE, S. E. WILSON, AND T. KOBARI. 2008a. A comparison of mesopelagic mesozooplankton community structure in the subtropical and subarctic Pacific Ocean. Deep-Sea Res. II **55:** 1615–1635.

———, M. W. SILVER, AND C. H. PILSKALN. 1997. The role of mesopelagic zooplankton in the community metabolism of giant larvacean house detritus in Monterey Bay, California. Mar. Ecol. Prog. Ser. **147:** 167–179.

———, B. A. S. VAN MOOY, K. O. BUESSELER, P. W. BOYD, T. KOBARI, AND D. M. KARL. 2008b. Bacterial vs. zooplankton control of sinking particle flux in the ocean's twilight zone. Limnol. Oceanogr. **53:** 1327–1338.

STRAILE, D. 1997. Gross growth efficiencies of protozoan and metazoan zooplankton and their dependence on food concentration, predator–prey weight ratio, and taxonomic group. Limnol. Oceanogr. **42:** 1375–1385.

SUESS, E. 1980. Particulate organic carbon flux in the oceans-surface productivity and oxygen utilization. Nature **288:** 260–263.

THIBAULT, D., S. ROY, C. S. WONG, AND J. K. BISHOP. 1999. The downward flux of biogenic material in the NE subarctic Pacific: Importance of algal sinking and mesozooplankton herbivory. Deep-Sea Res. II **46:** 2669–2697.

TRULL, T., K. BUESSELER, S. BRAY, C. MOY, F. EBERSBACH, C. LAMBORG, S. PIKE, AND S. MANGANINI. 2008. In-situ measurement of mesopelagic particle sinking rates and the control of carbon transfer to the ocean interior during the vertical flux in the global ocean (VERTIGO) voyages in the North Pacific. Deep-Sea Res. II **55:** 1684–1695.

VALDES, J. R., AND J. F. PRICE. 2000. A neutrally buoyant, upper ocean sediment trap. J. Atmos. Oceanogr. Tech. **17:** 62–68.

VOLK, T., AND M. I. HOFFERT. 1985. Ocean carbon pumps: Analysis of relative strengths and efficiencies in ocean-drive atmospheric CO_2 changes. Geophys. Monogr. **32:** 99–110.

WAITE, A., AND S. D. NODDER. 2001. The effect of in situ iron addition on the sinking rates and export flux of Southern Ocean diatoms. Deep-Sea Res. II **48:** 2635–2654.

WAPLES, J. T., C. BENITEZ-NELSON, N. SAVOYE, M. RUTGERS VAN DER LOEFF, M. BASKARAN, AND Ö. GUSTAFSSON. 2006. An introduction to the application and future use of [234]Th in aquatic systems. Mar. Chem. **100:** 166–189.

WASSMANN, P. 1990. Relationship between primary and export production in the boreal coastal zone of the North Atlantic. Limnol. Oceanogr. **35:** 464–471.

———, K. OLLI, C. WEXELS RISER, AND C. SVENSEN. 2003. Ecosystem function, biodiversity and vertical flux regulating in the twilight zone, p. 279–287. *In* G. Wefer, F. Lamy and F. Mantoura [eds.], Marine Science Frontiers for Europe. Springer Verlag.

WILSON, S. E., D. K. STEINBERG, AND K. O. BUESSELER. 2008. Changes in fecal pellet characteristics with depth as indicators of zooplankton repackaging of particles in the mesopelagic zone. Deep-Sea Res. II **55:** 1636–1647.

YU, E.-F., R. FRANCOIS, M. P. BACON, S. HONJO, A. P. FLEER, S. J. MANGANINI, M. M. RUTGERS VAN DER LOEFF, AND V. ITTEKOT. 2001. Trapping efficiency of bottom-tethered sediment traps estimated from the intercepted fluxes of [230]Th and [231]Pa. Deep-Sea Res. I **48:** 865–889.